THE ASTROPHYSICAL JOURNAL, 430:29–52, 1994 July 20

BIAS PROPERTIES OF EXTRAGALACTIC DISTANCE INDICATORS. III. ANALYSIS OF TULLY-FISHER DISTANCES FOR THE MATHEWSON-FORD-BUCHHORN SAMPLE OF 1355 GALAXIES

MARTIN FEDERSPIEL
Astronomisches Institut der Universität Basel, Venusstrasse 7, CH-4102 Binningen, Switzerland
ALLAN SANDAGE
The Observatories of the Carnegie Institution of Washington, 813 Santa Barbara Street, Pasadena, CA 91101
AND
G. A. TAMMANN
Astronomisches Institut der Universität Basel, Venusstrasse 7, CH-4102 Binningen, Switzerland
Received 1993 October 26; accepted 1994 January 21

ABSTRACT

The observational selection bias properties of the large Mathewson-Ford-Buchhorn (MFB) sample of galaxies are demonstrated by showing that the apparent Hubble constant incorrectly increases outward when determined using Tully-Fisher (TF) photometric distances that are uncorrected for bias. It is further shown that the value of H_0 so determined is also multivalued at a given redshift when it is calculated by the TF method using galaxies with different line widths. The method of removing this unphysical contradiction is developed following the model of the bias set out in Paper II. The model developed further here shows that the appropriate TF magnitude of a galaxy that is drawn from a flux-limited catalog not only is a function of line width but, even in the most idealistic cases, requires a triple-entry correction depending on *line width, apparent magnitude, and catalog limit.*

Using the distance-limited subset of the data, it is shown that the *mean* intrinsic dispersion of a bias-free TF relation is high. The dispersion depends on line width, decreasing from $\sigma(M) = 0.7$ mag for galaxies with rotational velocities less than 100 km s^{-1} to $\sigma(M) = 0.4$ mag for galaxies with rotational velocities greater than 250 km s^{-1}.

These dispersions are so large that the random errors of the bias-free TF distances are too gross to detect any peculiar motions of individual galaxies, but taken together the data show again the offset of 500 km s^{-1} found both by Dressler & Faber and by MFB for galaxies in the direction of the putative Great Attractor but described now in a different way. The maximum amplitude of the bulk streaming motion at the Local Group is $\sim$500 km s^{-1}, but the perturbation dies out, approaching the Machian frame defined by the CMB at a distance of $\sim$80 Mpc ($v \sim 4000$ km s^{-1}). This decay to zero perturbation at $v \sim 4000$ km s^{-1} argues against existing models with a single attractor at $\sim$4500 km s^{-1} (the Great Attractor model) pulling the local region. Rather, the cause of the perturbation appears to be the well-known clumpy mass distribution within 4000 km s^{-1} in the busy directions of Hydra, Centaurus, Antlia, and Dorado, as postulated earlier (Tammann & Sandage 1985).

Subject headings: distance scale — galaxies: distances and redshifts — methods: statistical

1. INTRODUCTION

This series of papers is concerned with procedures to detect and correct systematic errors in photometric distances of galaxies determined using any of a variety of methods. The systematic errors arise because the mean luminosity of a homogeneous set of galaxies drawn from a flux-limited catalog increases with increasing distance. The bias properties of such ideal samples began to be isolated in what could be considered the first (although unnumbered) paper of this series (Sandage, Tammann, & Yahil 1979, hereafter STY79) using the strictly flux-limited sample of the Revised Shapley-Ames Catalog (Sandage & Tammann 1981).

In the present paper we extend the analysis of Paper II (Sandage 1994b, hereafter Paper II) on the bias properties of distances derived from the Tully-Fisher (TF) method. We analyze here the TF distances determined by Mathewson, Ford, & Buchhorn (1992a, hereafter MFB) for their large sample of 1355 galaxies.

Our purposes are (1) to demonstrate in § 3 that the MFB sample, uncorrected for observational selection bias, leads to the unphysical situation of a Hubble constant that apparently increases outward and, in addition, is multivalued at a given redshift for different line widths and different apparent magnitudes, or, alternatively, is multivalued at different line widths at a fixed redshift; (2) to demonstrate in § 4, using the Spaenhauer diagram (absolute magnitude versus redshift), the nature of the selection bias leading to this contradiction; (3) to show in § 5 how to use the data to define a bias-free slope to the TF relation by considering the subsample of the total MFB sample that is *distance-limited*; (4) to discuss in § 6 the individual corrections for selection bias that must be applied to the MFB sample; (5) to come back in § 7 to the example in § 3, presenting the results after applying the selection bias corrections we worked out in § 6, showing how the contradiction is resolved; (6) to demonstrate in § 8 how the corrected Hubble diagram for the bias-corrected sample shows no evidence for deviations from a pure linear Hubble flow except for the known Virgocentric infall and the large-scale motion of the "local" region

($v < 4000$ km s^{-1}) shown by the cosmic microwave background (CMB) dipole; and (7) to set out in § 9 the main conclusion of this paper, emphasizing the need to identify and to correct the systematic errors of distances for field galaxies due to observational selection bias before such cosmological parameters as the Hubble constant and any streaming motions on top of the cosmological flow can be found by photometric methods.

2. THE MATHEWSON-FORD-BUCHHORN DATA SAMPLE

Galaxies in the large sample studied by MFB were selected in a number of ways, and therefore form neither a strictly flux-limited nor a volume-limited sample. Most of the galaxies were selected from the ESO-Uppsala survey (Lauberts 1982), where the selection limit is on diameters of 1'.0. Only galaxies of types Sb–Sd are included in the MFB sample, with the additional restriction that they have angular diameters greater than 1'.7, well above the ESO limit. In the region near Hydra and Centaurus, and in a few other regions as well, galaxies in the supergalactic plane survey of Dressler (1988) with redshifts[1] greater than 7000 km s^{-1} were also included.

The evidently heterogeneous nature of the selection criteria (by diameter rather than apparent magnitude, by Hubble types with wide ranges in surface brightness, by redshift in some cases, etc.) makes many of the analytical methods of corrections for selection bias highly formal and, therefore, often inappropriate. Such methods can only be used in their elegant formality when the biased samples are chosen by strict criteria, and on the assumption of constant space density. In the absence of such rigor, the formal solutions generally fail to give back reality. Of course, their great structural beauty often speaks for them, but their inappropriateness is just as often hidden.

On the other hand, the empirical methods developed earlier (STY79; Sandage 1988b, hereafter S88b) and by Sandage (1994a, b, hereafter Papers I and II) permit detection of the bias directly via Spaenhauer diagrams. These diagrams as defined and used in Papers I and II, made by plotting individual absolute magnitudes against individual redshifts, generally contain all the information needed to correct for the effects of the bias even if the sample has not been chosen by rigid criteria.

In addition to the 1094 field galaxies, the MFB sample contains 261 galaxies assigned to clusters (Fornax, Sculptor, Centaurus, Antlia, etc.) which we do not use in this paper. The catalog also contains information on position, morphological type, diameters, I-band magnitudes as observed, and I-band magnitudes statistically corrected for the small absorption effects of inclination and Galactic extinction. Redshifts, radio line widths, optical maximum rotational velocities, and other galaxy properties are also listed by MFB.

For the present investigation, the photometric data, the redshifts, and the inclination-corrected rotational velocities are used as defined at *half the* 21 cm *line widths read at the* 50% *level* if radio data are used, or the maximum observed velocities obtained from the optical data.

The heliocentric redshift velocities are transformed to redshifts relative to the Local Group using the precepts of the RSA (Sandage & Tammann 1981, 1987) based on the solution by Yahil, Tammann, & Sandage (1977). These redshifts are then variously transformed (§ 8) into the Virgocentric frame (Kraan-Korteweg 1986b) and also to the frame of the CMB in later sections in separate discussions of the several velocity frames that are relevant for cosmology.

The most secure analysis is with a subsample cut rigorously at apparent magnitude $I = 12.5$, which we consider to be strictly flux-limited. The systematic bias properties of this subsample are then seen in all their starkness because of this rigorous selection by flux limitation. The evidence that this subsample is flux-limited is the following.

There are 813 objects with $I = 12.5$ mag and brighter in the MFB catalog. Of these, 808 have diameters of 1'.5 or larger. The ESO catalog, from which most of the MFB sample was chosen, is said to be complete for all galaxies with diameters of 1'.0 and larger. Hence, the MFB list is a flux-limited sample when restricted to galaxies with $I < 12.5$. To carry the argument further, searching for a possible incompleteness factor, of the 813 galaxies with $I = 12.5$ and brighter, 762 have diameters larger than 1'.7, well above the ESO catalog limit. Hence, the bright sample used here is very close to an ideal, complete, *flux-limited* list.

3. A "NAIVE" APPLICATION OF THE TULLY-FISHER METHOD TO MAP THE APPARENT (INCORRECT) LOCAL VELOCITY FIELD VIA THE RELATIVE HUBBLE CONSTANT

The MFB photometric data are in the I-band. Because too few galaxies with fundamental Cepheid distances exist to determine adequately the bias-free TF slope (the slope that applies to a distance-limited sample), MFB used the data for Fornax Cluster spirals to determine such a slope. Instead, we follow an equivalent precept here (see § 5 and Fig. 7) using only the *distance-limited* field galaxy subset of the total MFB sample. The aim is to set out the biased consequences of applying a normal TF analysis to a non–distance-limited sample to see the bias properties and, therefore, to identify the contradictions directly.

The TF slope adopted by MFB from the Fornax Cluster data is $dM_I/d \log v_{\rm rot} = -7.96$. Our analysis in § 5 using the distance-limited subsample of the MFB catalog gives the nearly identical slope of $dM_I/d \log v_{\rm rot} = -7.74$.

The TF relation (with the MFB slope imposed) can be calibrated by adopting an arbitrary[2] relative kinematic distance scale based on $H_0 = 50$ km s^{-1} Mpc^{-1}. Calibration of the TF equation used by MFB to predict distances in redshift units can be changed into the absolute magnitudes used here by

$$M_I = -7.96 \log v_{\rm rot} - 4.46 . \quad (1)$$

This follows from $I = -7.96 \log v_{\rm rot} + 27.68$ given in the description of column (12) of MFB for the calibration (in km

[1] The terms "redshift" and "(expansion) velocity" are used here interchangeably, although in cosmology the term "velocity" is meaningless, the "expansion" being the time variation of the metric scale factor via the famous Lemaître equation, not a "Doppler" effect. Of course, the fraction of the redshift that reflects *peculiar* motions is presumed to mean real Doppler velocities.

[2] Because the deliberations in this paper are concerned only with the distortion of a *relative* distance scale (based on an arbitrary value of $H_0 = 50$ km s^{-1} Mpc^{-1}) by the presence of bias, the absolute calibration is irrelevant. Our method in the later sections is to devise corrections only to a *relative* scale that has (incorrectly) become nonlinear because of a naive application of the TF relation, fouled by selection bias at each redshift and each line width. The resulting corrections recover the linearity which we assume when we calculate the initial Spaenhauer diagrams (Figs. 5 and 6 below). We require only that we recover the same zero point for the final relative scale that was assumed ab initio. The proof that the method is not circular is given in Paper II and in § 7.2 of this paper.

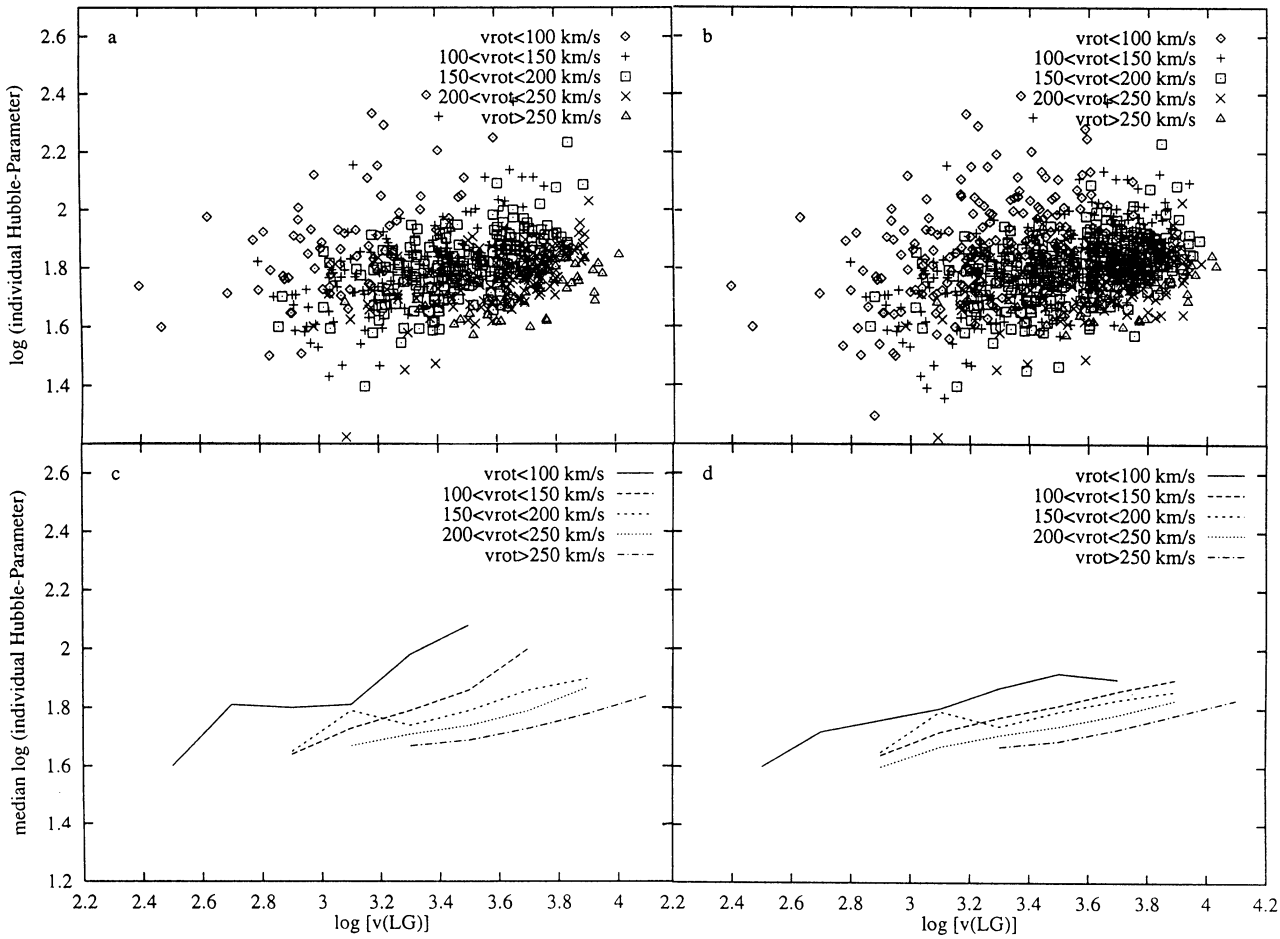

FIG. 1.—Individual Hubble velocity-distance ratios as a function of redshift for different subsamples of the MFB total sample, coded according to rotational velocities: (*a*) for all galaxies brighter than $I = 12.5$ mag (often called the "bright" sample, which we assert is closely flux-limited) and (*b*) for the MFB total sample (clusters excluded). Individual TF distances are calculated from the Tully-Fisher relation in eqn. (1) based on the MFB Fornax Cluster slope but zero-pointed to correspond to $H_0 = 50$. Panels *c* and *d* are the same as panels *a* and *b*, except that mean lines are used for the individual Hubble ratios, h_i, for each rotational velocity bin. The multivalued nature of the Hubble ratios, depending on redshift, rotational velocity, and apparent magnitude, shows the impossible contradiction resulting from using the TF method naively in this way to determine photometric distances.

s^{-1}) via the Fornax Cluster, adopting the redshift of Fornax to be 1340 km s^{-1} and $H_0 = 50$ km s^{-1} Mpc^{-1} (as throughout this paper). With these parameters, the Fornax Cluster modulus is $m - M = 32.14$. The constant term in equation (1) follows by noting that $27.68 - 32.14 = -4.46$.

Individual distance moduli, $(m - M)_I$, have been calculated for all galaxies in the MFB sample using equation (1) with the v_{rot} values listed by MFB (corrected for inclination) and with their adopted "total *I*-band magnitudes corrected for internal and external extinction and *K* dimming." From these naively calculated raw distances, with no account taken of bias problems, the individual Hubble ratios, v_i/d_i for galaxy *i*, follow for all galaxies in the sample. The results are shown in Figure 1 for two cuts of the sample by apparent magnitude, each separated into bins of rotational velocity (i.e., LW/2), marked by different symbols.[3]

The most striking feature of Figures 1*a* and 1*b* is the apparent increase of the mean Hubble ratios with distance, ranging in Figure 1*b* between the extremes of $\langle h_i \rangle \sim 40$ km s^{-1} Mpc^{-1} and $\langle h_i \rangle \sim 80$ km s^{-1} Mpc^{-1} at various distances. Such an increase of the effective Hubble parameter with distance would not necessarily be a contradiction per se. An increase could, rationally, exist in nature, if this were the only gross information available (de Vaucouleurs & Peters 1986; Giraud 1985, 1986a, b, c; Tully 1988). However, buried in the panels of Figure 1 is the decisive contradiction, showing beyond doubt that the Hubble constant does not increase outward (Papers I and II).

[3] It is often asked whether redshifts that are corrected to the centroid of the Local Group (Humason & Wahlquist 1955; Yahil et al. 1977), as listed in col. (20) of the RSA and labeled "LG" in Figs. 1–14 of this paper, are as appropriate as the *v*(220) redshifts that are referred to the Virgocentric kinematic frame (Kraan-Korteweg 1986a, b for the model, and Tammann & Sandage 1985 for the adopted "infall" velocity of 220 km s^{-1}), or whether spurious effects are introduced simply by using *v*(LG).

To test this, the equivalent of Figs. 1 and 3, but using *v*(220) redshifts, are shown in Figs. 20 and 21 in the Appendix. The principal bias properties of each diagram using either *v*(LG) or *v*(220) are the same. Although minute details differ, the thrust of the argument in this and in Papers I and II is not vulnerable to riposte for this reason of kinematic frame alone.

It should further be noted that the observed multivaluedness of the correlations in Figs. 1 and 3 here are just those predicted by the model in Paper II (Figs. 4, 7, 8, and 16), and therefore, if that model is correct, these correlations must be found in the data if bias exists. Hence, turning the argument around, we can say that because these multivalued relations are seen so well in Figs. 1 and 3 using *v*(LG), the Local Group centroid is not so far from the ideal Machian kinematic frame as to destroy the expected correlations. The reason for this important point is developed in § 8 of this paper.

The contradiction is seen from the *different* apparent values of h_i in Figures 1*c* and 1*d* for different line widths *at a given redshift. Or, conversely, the derived Hubble ratios are multivalued at a given line width depending on the redshift.* There is also a strong dependence on the adopted limiting magnitude of each subsample of the total MFB sample.

The evidence is set out in Figures 1*c* and 1*d*, showing the same samples as in Figures 1*a* and 1*b* but using mean (ridge) lines. These are calculated from the median values of the data for a particular interval of the abscissa (typically 0.1 dex, rarely 0.2 dex). Each interval gave one point in the middle of the interval. The points were then connected, giving the ridge lines.

Figures 1*a* and 1*c* show the derived Hubble ratio versus distance (in redshift units along the abscissa) for the bright MFB sample restricted to apparent magnitudes brighter than $I = 12.5$. The Hubble ratios are clearly different from those in Figures 1*b* and 1*d* that hold for the total sample, which, on average, is fainter. Hence, the apparent Hubble ratio also depends on the nature of the sample, which, of course, is a further contradiction.

A different representation of the data is set out in Figure 2, where the axes are rotational velocity and individual Hubble parameter. The generator of the family in Figure 2 is redshift.

The multivalued nature of the Hubble ratio with (*a*) limiting magnitude of each subsample, (*b*) the value of v_{rot}, and (*c*) redshift, evident in Figures 1 and 2, is clearly unphysical. The effects are artifacts of an analysis made by using equation (1) in an intuitive, but incorrect, way. However, the error is widespread enough in the literature that it would be unfair to identify its heresiarch in North America.

Note that the multivalued properties of the correlations in Figures 1 and 2 are just those expected from the model set out in Paper II if observational selection bias is present in non–distance-limited samples (Paper II, Figs. 8, 14, 15, and 16). The methods of removing the contradictions by correcting the effects of bias are the subjects of this paper.

4. THE ASSUMPTION OF A LINEAR EXPANSION AND THE SPAENHAUER DIAGRAM

4.1. *A Calculated Tully-Fisher Relation Based on a Linear Expansion*

To understand why equation (1) has led to the impossible results in § 3, we assume, for illustration, that the expansion field is perfectly linear with negligible peculiar motions. Arbitrarily using $H_0 = 50$, we have calculated the kinematic (redshift) distance $d = v_{redshift}/H_0$, the distance modulus $m - M = 5 \log d - 5$, and from that the absolute magnitude M_I using the apparent, fully corrected, I-band magnitude for each galaxy listed by MFB. The resulting M_I values, plotted

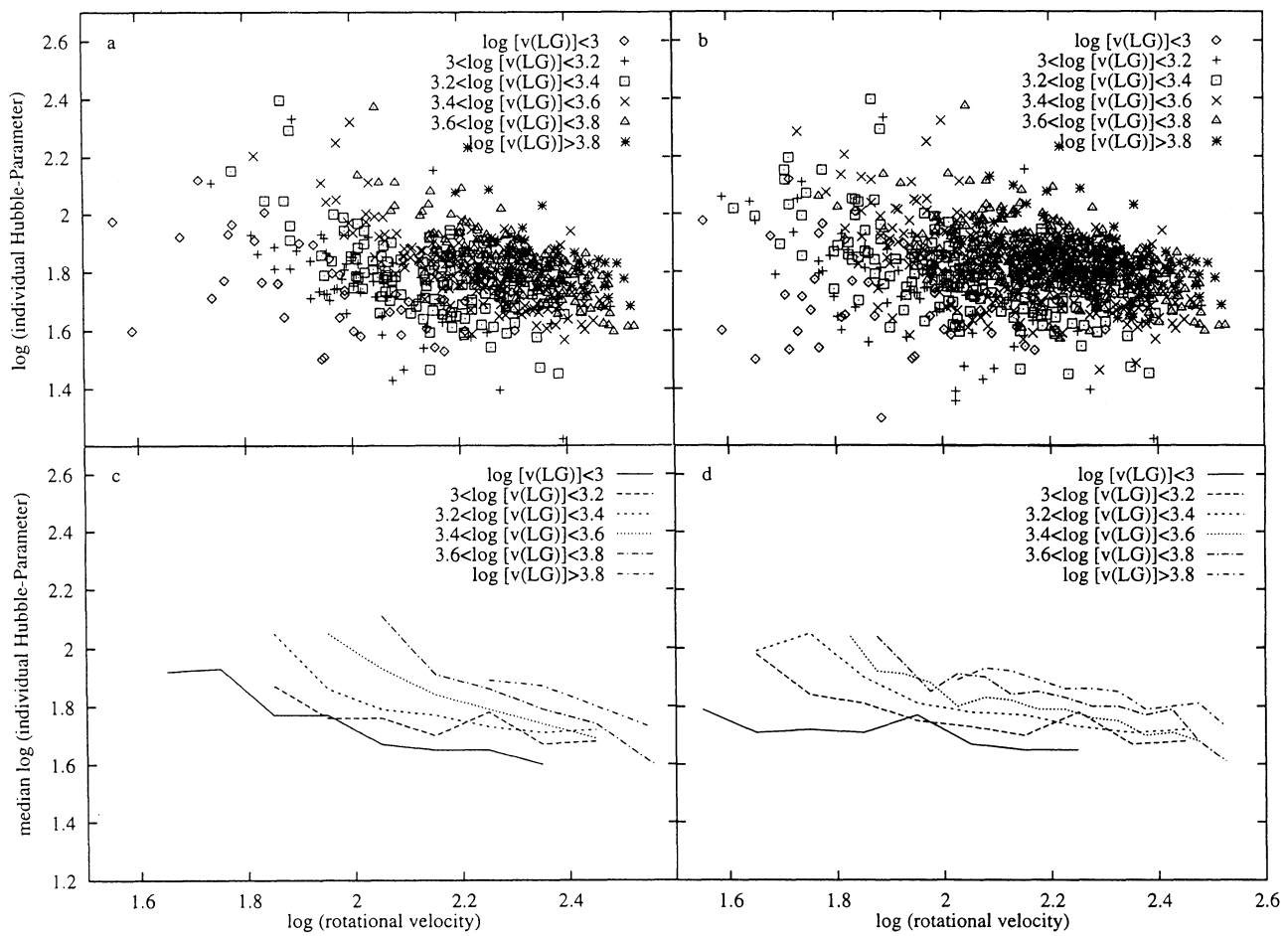

FIG. 2.—Same data as in Fig. 1, but in a different representation. Rotational velocity is the independent variable, and log redshift is the generator of the family. The same contradiction as in Fig. 1 is that H_0 is multivalued at a given redshift for different rotational velocities. The cause is severe selection bias.

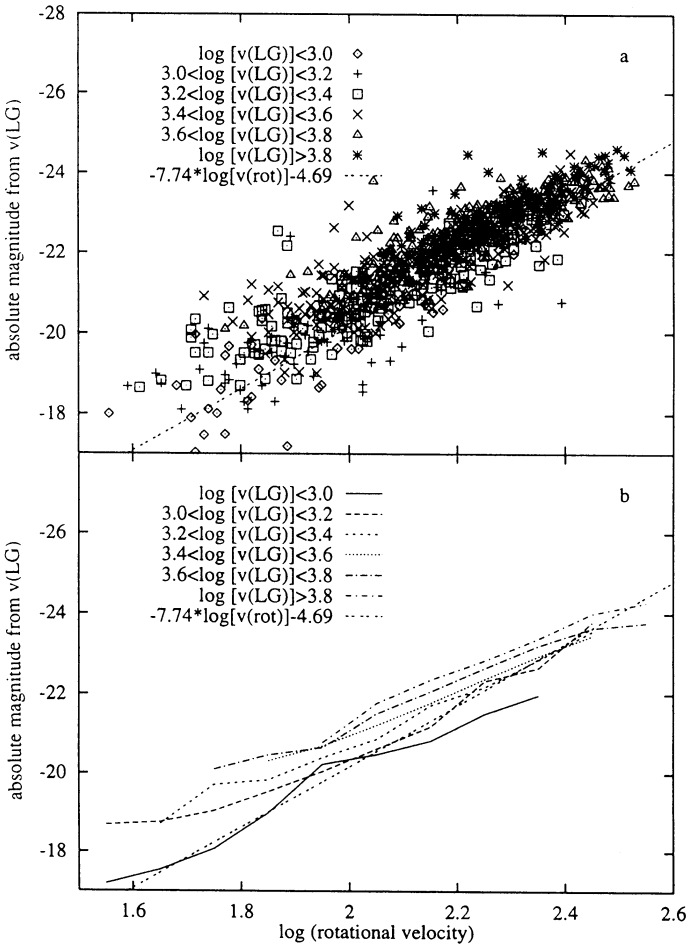

FIG. 3.—(*a*) TF relation for the "total" MFB sample using kinematic absolute magnitudes ($H_0 = 50$ km s^{-1} Mpc^{-1}) as ordinate and observed rotation velocities (i.e., LW/2) as abscissa. The drawn line is the bias-free TF relation of eqn. (4*b*), based on $H_0 = 50$. The offset of the line below the mean of the sample is a result of the observational selection bias. Its size of 0.7 mag is consistent with the expected (formal) Malmquist effect that $M_0 - M(m) = 1.39\sigma^2$ if $\sigma(M) = 0.7$ mag. We contend that the neglect of the offset in its various disguises as functions of redshift and rotational velocity is a primary cause of the current debate on the value of H_0 using the TF method. (*b*) Mean lines for different redshifts from the data, now restricted to the $I < 12.5$ mag bright sample. The systematic variation of the positions of the mean lines with increasing redshift was discovered empirically by Kraan-Korteweg, Cameron, & Tammann (1986, 1988). This is the decisive clue that observational selection bias, uncorrected, controls the determination of H_0 using the TF method. The behavior of the mean lines for different line widths is closely the same as predicted from the bias model in Paper II (Figs. 4 and 7).

against the corresponding rotational velocities (half the radio line widths) give the Tully-Fisher relation in Figure 3*a*. A least-squares line fitted to the data has the equation

$$M_I = -6.83 \log v_{\rm rot} - 7.12 , \qquad (2)$$

with a standard deviation of $\sigma(M) = 0.59$ mag.

The dot-dash line near the bottom of the distribution in Figure 3*a* is not equation (2) but is the *bias-free* relation of equation (4*b*) set out later. The difference between equations (2) and (4*b*), and therefore the difference in the position of the dot-dash line and a mean line through the Figure 3 data, is, of course, due to the effect of the gross Malmquist bias.

We believe most of the large scatter in Figure 3*a* is intrinsic because the compounded observational errors in magnitude, line width, and inclination can hardly be as large. The only alternative would be to invoke peculiar motions. However, this is improbable, seen from at least four clues to the case:

1. The deviations in Figure 3*a* are much larger for galaxies with the smallest bin of $v_{\rm rot}$ [$\sigma(M) = 0.9$ mag], and as small as $\sigma(M) = 0.43$ mag for galaxies with the highest $v_{\rm rot}$. If the dispersions were due to peculiar motions, they would, therefore, have to be a function of galaxy size (mass, absolute magnitude), which is absurd. Moreover, to explain $\sigma(M)$ as large as 0.9 mag, the peculiar motions would have to be as large as $\sim 50\%$ of the true recession redshift, which is known to be incorrect (Paper II, § 2.2, and § 8 of this paper).

2. The slope of -6.83 in equation (2) is considerably flatter than the value of -7.96 found in the Fornax Cluster by MFB, and by us (§ 5, eqs. [4*a*] and [4*b*]) for the unbiased relation in Figure 7. This shows that the TF relation is sensitive to the sample selection, being different for each sample. This clearly must be due to selection bias (it follows the prediction in Fig.4 of Paper II) rather than to real streaming motions, because if such motions are *real*, they *must be independent of the sample used to determine them.*

3. Related to item 2 is the fine structure buried in Figure 3*a* as a function of redshift. This can be isolated as follows: Divide the complete MFB sample (or subsamples binned by apparent magnitude) into intervals of rotational velocity. Then bin each sample into different redshift intervals, and plot each group separately in the equivalent of Figure 3*a*. *The result is that the mean lines become progressively brighter with increasing redshift, and the slopes become steeper.*

This phenomenon was discovered empirically by Kraan-Korteweg, Cameron, & Tammann (1986, 1988) in the TF sample of Aaronson et al. (1982). The result for the MFB $I < 12.5$ mag subsample here is shown by the mean (ridge) lines in Figure 3*b*. The stacking of these mean lines according to redshift, and the accompanying progressive change of slope, are well shown. It is in fact, precisely the prediction from the bias model developed in Figures 4 and 7 of Paper II. The point is that all details of these predictions are seen in the *real* MFB data set out in Figure 3*b*. Fine structure in such detail relative to the model would be absent if the spreads were due to peculiar motions.

4. The signature of peculiar motions in Spaenhauer diagrams such as Figures 5 and 6 below would be decreased scatter at higher redshifts because $\Delta v_{\rm peculiar}/v_{\rm cosmic}$ *decreases* with increasing distance. The observed nature of the scatter in all the Spaenhauer diagrams set out in later sections is just the reverse, again showing that peculiar motions cannot be the explanation of the scatter in Figure 3*a* but rather that the scatter is intrinsic.

4.2. *The Spaenhauer Diagram for the Total MFB Sample*

The Spaenhauer diagram (SD), where absolute magnitudes are plotted against redshift, is a powerful tool with which to visualize selection effects in flux-limited samples. The SD for the total MFB sample is shown in Figure 4, plotted against log redshift, again using $H_0 = 50$. The sample is separated into six bins according to apparent magnitude.

All of the bias properties discussed in Papers I and II found by adding a fainter sample are seen in Figure 4, showing the lower limit lines that become fainter as each progressively fainter sample is considered. The relation between absolute

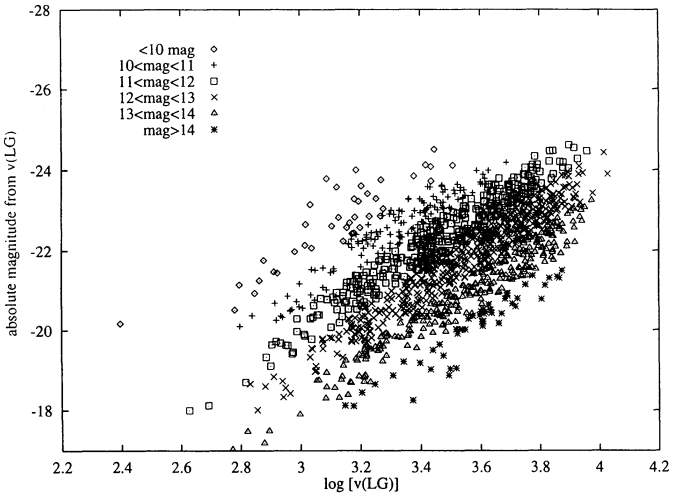

FIG. 4.—Absolute magnitudes, calculated from redshifts (based arbitrarily on $H_0 = 50$) as a function of distance (the Spaenhauer diagram) for the MFB "total" sample. The data are stacked according to apparent magnitude. Lines of constant apparent magnitude follow eq. (3). The sharp separation by apparent magnitude is the decisive signal that observational selection bias is present. The method of detection of bias is to add a fainter sample, as is done here, and to see the progressive change in the topology of the diagram as the fainter subsamples are added.

and apparent magnitudes at redshift v is, of course,

$$M = -5 \log v_{\text{redshift}} - 16.5 + m \qquad (3)$$

(the constant term depending on $H_0 = 50$), defining each of the very sharp separations according to apparent magnitude in Figure 4.

This Spaenhauer diagram reveals many of the basic problems with flux-limited samples. Very luminous galaxies ($M < -23$ on the arbitrary scale of $H_0 = 50$) are rare, and therefore are not observed nearby because there is only a small probability of finding them in the small available volume. As we go farther out, the volume grows and the high end of the luminosity function is observed. Objects of high luminosity have bright apparent magnitudes even at large distances, and therefore have a good chance to be included above the flux limit of flux-limited catalogs. They are found in the upper right-hand part of the Spaenhauer diagram.

Intrinsically fainter objects at the same distance have fainter apparent magnitudes and may not fulfill the apparent magnitude criterion of the catalog. Therefore, no objects are found in the lower right-hand part of the diagram. But if we add an additional sample with a fainter limiting magnitude, the lower right-hand part below the original magnitude limit will be populated too. This is the effect seen in Figure 4.

As mentioned previously, the MFB sample is neither volume-limited nor flux-limited because the ESO-Uppsala survey (Lauberts 1982), which is the main source of the MFB catalog, is limited by apparent (angular) diameter. Hence, the edge of the lowest luminosity end of the Spaenhauer diagram in Figure 4 is not sharp as in, say, Figures 2 and 11 of Paper I.

4.3. *Spaenhauer Diagrams for Different Rotational Velocities*

To demonstrate the bias effects inherent in the Tully-Fisher method as it is usually applied, it is helpful to plot separate Spaenhauer diagrams for several rotation velocity intervals. The five panels of Figure 5 show five subsamples corresponding to rotational velocity intervals of $\Delta v_{\text{rot}} = 50$ km s^{-1} for the total MFB sample (but excluding cluster galaxies). A lower apparent magnitude limit line for $I = 14$ mag is shown in each panel to guide the eye, although the samples are not actually flux-limited. To better approximate a more strictly flux-limited sample, we limit the MFB sample to $I = 12.5$ mag in the five similar Spaenhauer diagrams in Figures 6*a*–6*e*.

Each of the five panels in both Figures 5 and 6 is plotted with the same positioning of the zero points for the ordinate, so that the progression toward brighter absolute magnitudes can be seen by the upward displacements as the rotational velocities change from less than 100 km s^{-1} to greater than 250 km s^{-1}. This brightening is simply the mean (ridge-line) Tully-Fisher relation.

From these diagrams we can derive the mean absolute magnitudes needed to remove the contradictions at each rotational velocity and at each redshift by the method discussed in Paper II, now described again here.

For definiteness, assume that the true (i.e., the volume-limited) luminosity function is Gaussian, but in fact the form of the luminosity function can be arbitrary because our ultimate bias corrections (Fig. 8) are determined empirically rather than analytically later in this section.

The mean absolute magnitude of any distance-limited subsample is, of course, equal to the peak absolute magnitude of the Gaussian fitted to the observed luminosity function for galaxies at all distances within which the sample is complete, i.e., where the sample is indeed distance-limited. Objects fainter than the apparent magnitude limit of the subsample have not entered the catalog and do not contribute to the observed luminosity function. Therefore, it is not permitted to use the peak of the true luminosity function for distances *where the lower part of the luminosity function is incomplete.*

In the manner described in Paper I (Fig. 3), the upper and lower envelopes in a SD can be calculated in such a way that only one galaxy is expected in the distribution, given (1) the position of the apex of the SD configuration [i.e., M_0(LW)] and (2) the value of the intrinsic dispersion of the true luminosity function. The SD envelope configurations from a straightfoward calculation such as that in Paper I (Table 1 and Fig. 8 there) are shown in Figures 5 and 6 here.

The "best-fitting" SD envelope configurations in the different panels of Figures 5 and 6 were determined by eye, using the template curves of Paper I (Fig. 3). The widths of the configurations depend, of course, on the luminosity scatter $\sigma(M)$ within a given rotational velocity interval. The absolute magnitude of the apex, $M_0(v_{\text{rot}})$, is the *ridge-line* absolute magnitude of the unbiased TF relation determined in the objective calculation set out below in § 5. Having established the unbiased $\langle M_0(\text{apex})\rangle$ magnitudes for different rotational velocities in this way (eq. [4b] derived later in § 5), the appropriate template from Paper I has then been fitted to the observed data points by a horizontal shift in Figures 5 and 6.

The mean absolute magnitudes, $\langle M(v_{\text{rot}}, \text{redshift})\rangle$, in the *flux-limited* part of the sample are determined by averaging the data. They are shown in Figures 5 and 6 by lines threading the middle of the configurations. These, of course, are always brighter then the $M_0(v_{\text{rot}})$ apex magnitude. It is this difference between M_0 and $M(v_{\text{rot}}, \text{redshift})$ caused by the selection effects, that we must calibrate out if selection bias is to be removed.

The redshift at which the sample changes from being volume-limited to being flux-limited is where the apparent magnitude limit line intersects the curved lower envelope line. *This redshift can always be determined empirically from the rele-*

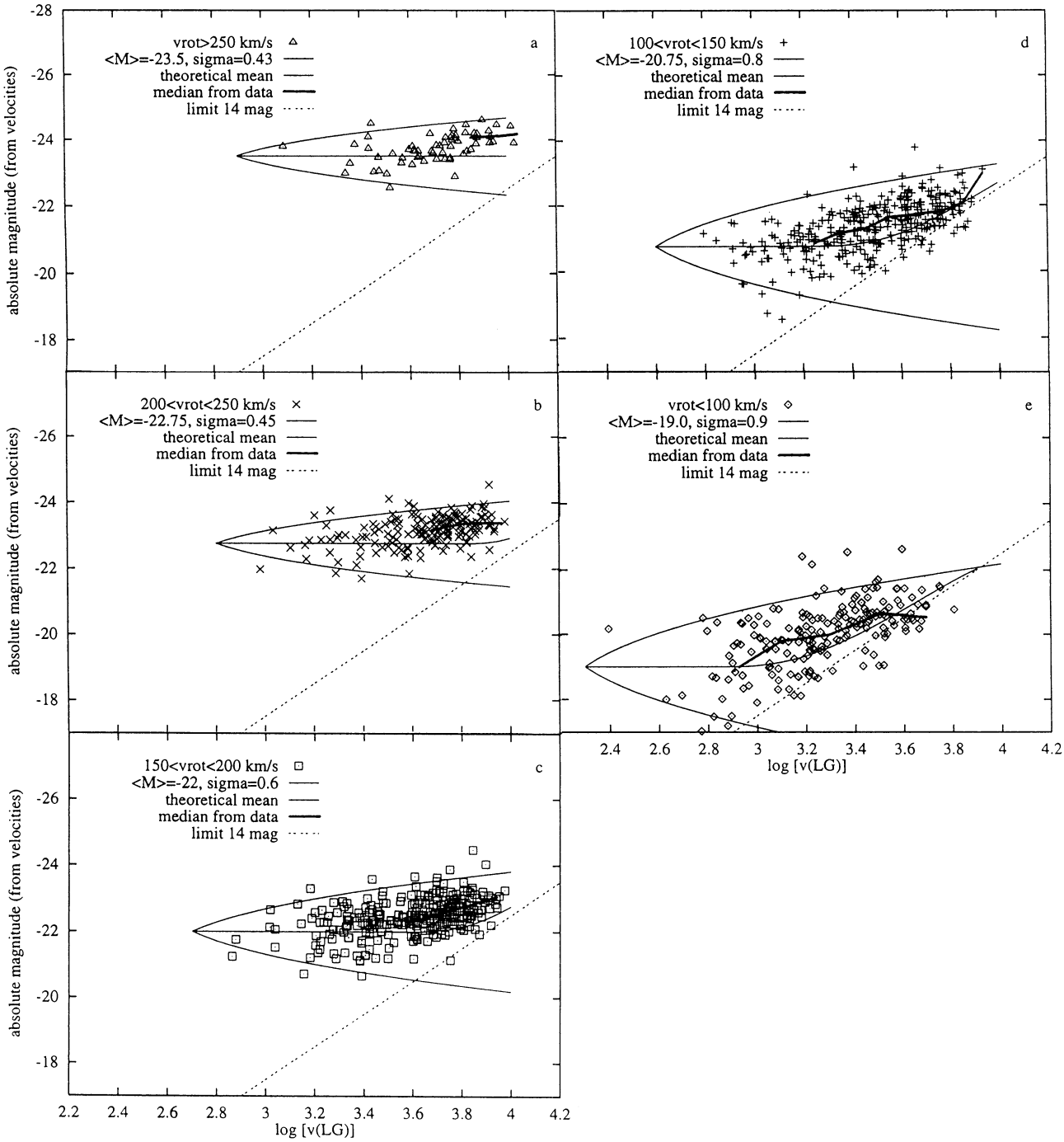

FIG. 5.—Spaenhauer diagrams for different rotational velocity bins for the "total" sample of MFB (cluster galaxies not included): (*a*) $v_{rot} > 250$ km s^{-1}, (*b*) $200 < v_{rot} < 250$ km s^{-1}, (*c*) $150 < v_{rot} < 200$ km s^{-1}, (*d*) $100 < v_{rot} < 150$ km s^{-1}, and (*e*) $v_{rot} < 100$ km s^{-1}. Envelope lines are drawn surrounding the permitted area where galaxies should be found, calculated using Gaussian luminosity functions with the marked dispersions and mean absolute magnitudes, M_{apex}, for the five rotational velocity bins. The line of apparent magnitude limit $I = 14$ is added to guide the eye. The mean absolute magnitude, $M(m)$, per redshift interval, becomes brighter outward as the apparent magnitude limit cuts the lower part of the luminosity function.

vant Spaenhauer diagram, provided that the apparent magnitude limit of a catalog is reasonably well defined. Just as obviously, the horizontal position of the apex in each SD (i.e., the redshift of the apex) is determined by the space density of the objects considered. For instance, a shift $\Delta \log v_{apex} = 0.4$ to the right allows for an increase in the space density of a factor of 15.8.

Several facts are obvious from Figures 5 and 6.

1. Luminous galaxies with high rotational velocities suffer less from selection effects than intrinsically fainter galaxies because the intersections between the apparent magnitude limit and the lower envelope occur at much larger distances for

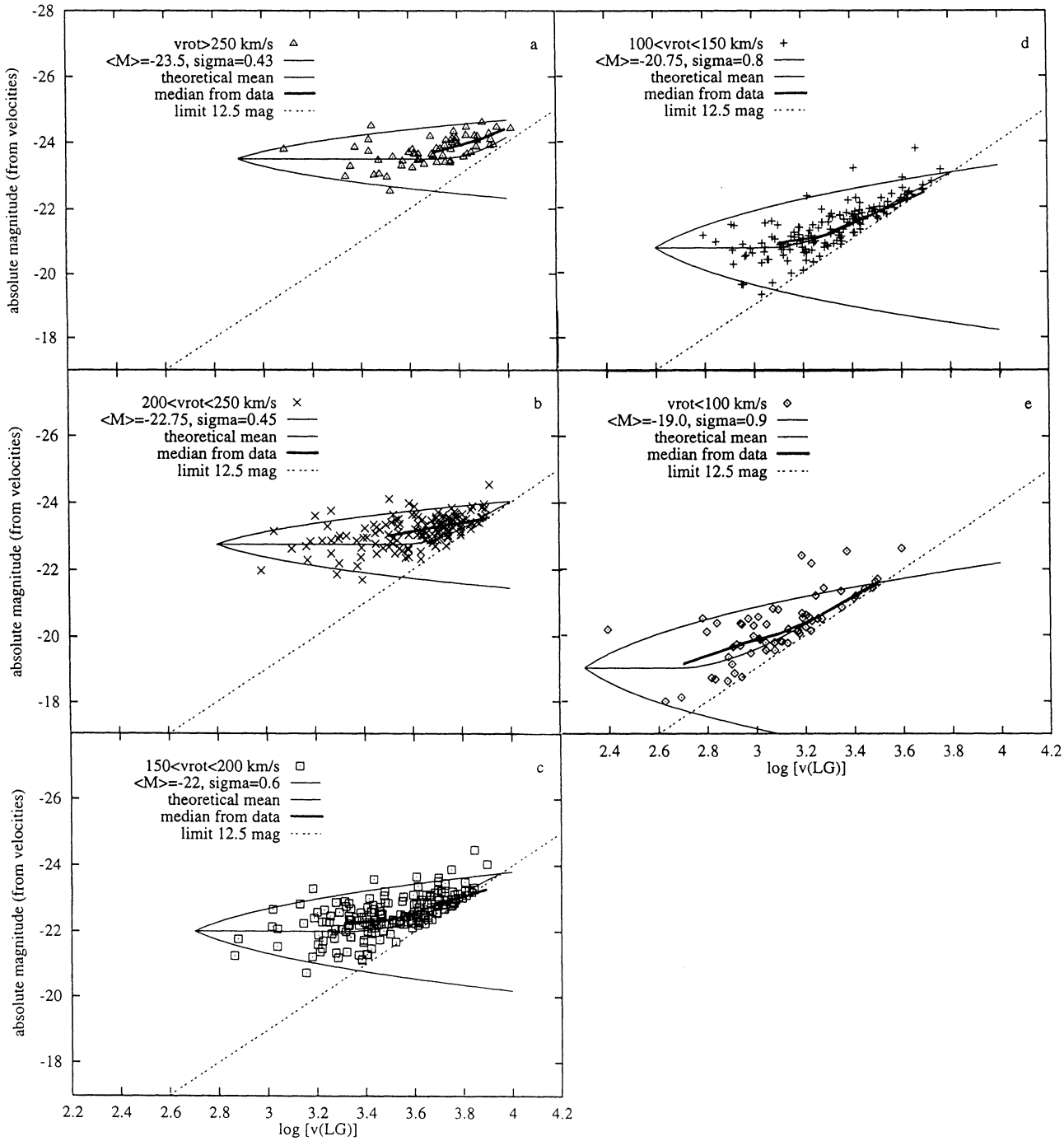

FIG. 6.—Separate Spaenhauer diagrams with envelope lines as in Fig. 5, but for the bright subsample cut rigorously at $I < 12.5$ mag (cluster galaxies excluded). The mean absolute magnitude, $M(m)$, per redshift interval, increases progressively outward, i.e., *is a function of redshift* as the apparent magnitude limit cuts the lower part of the luminosity function. This defines the specific corrections that must be applied to the data to correct for selection bias.

the luminous galaxies. (This point is only partially compensated for by the next point.)

2. Luminous galaxies are rare and are therefore only observed in a huge volume. As a consequence, the apex position is shifted to the right in the relevant SD compared with the apex position of intrinsically fainter galaxies.

3. The dispersion of the luminosity function decreases significantly with increasing rotational velocity, viz., $\sigma(M) = 0.9$ mag for $v_{\rm rot} < 100$ km s^{-1} and $\sigma(M) = 0.43$ mag for the fastest rotators. (The true dispersion is somewhat smaller because of the finite $v_{\rm rot}$ interval in each of the Spaenhauer configurations in the different panels of Figures 5 and 6. The contribution to the dispersion by the interval width can be roughly estimated from $v_{\rm rot}$ and eq. [4b] below. The remaining intrinsic scatter then becomes $\sigma(M) \sim 0.35$ mag for spirals with $v_{\rm rot} > 250$ km s^{-1} and $\sigma(M) \sim 0.7$ mag for galaxies with $v_{\rm rot} < 100$ km s^{-1}.)

In § 8 below, it will be found that the linear expansion may be smoother in the directions away from the "Great

Attractor" than toward it. It was therefore tested whether $\sigma(M)$ was smaller away from than toward the putative Great Attractor. No effect could be detected.

4. The different subsamples of v_{rot} do not share a common apparent magnitude limit in the MFB sample. There are very few objects with apparent magnitudes fainter than $I = 13$ for $v_{rot} > 250$ km s^{-1}, but many objects fainter than $I = 14$ mag with $v_{rot} < 100$ km s^{-1}. The probable explanation is that the selection criteria in the complete MFB sample are based on *angular diameter* rather than apparent magnitude. Because the surface brightness is a strong function of Hubble type *and therefore of rotational velocity* (Sd galaxies are of low surface brightness and of low v_{rot}; see Fig. 10 of MFB), there is a very strong selection effect against apparently faint high surface brightness galaxies (*which have high rotation velocity*) because they would have angular diameters smaller than the selection cutoff at 1'.5. Because of this added selection effect, we analyze a subsample (henceforth the "bright" sample) of the MFB catalog, cut at $I = 12.5$ mag, as our alternative list throughout this paper, on the assumption that this bright limit defines a more closely flux-limited sample, as justified earlier. In all the following, the "total" sample is to comprise all 1094 MFB galaxies that are not assigned to clusters.

5. CONSTRUCTION OF AN UNBIASED TULLY-FISHER RELATION

The first step on the way to the determination of Tully-Fisher distances that are free from selection bias is the construction of an unbiased ridge-line (mean) TF relation. The recipe for how to proceed is evident by considering the separate SD for the different rotational velocities (Figs. 5*a*–5*e* and 6*a*–6*e*).

Figure 7 shows the TF diagram (kinematic absolute magnitude on the arbitrary distance scale of $H_0 = 50$ versus rotational velocity) for all galaxies in the MFB sample (excluding cluster galaxies) in the bias-free regions. These are noncluster field galaxies to the left of where the apparent magnitude limit line intersects the lower envelope of the relevant Spaenhauer configurations. A least-squares fit to the data (*including* objects that are in the bias-free regions and also in the direction toward the "Great Attractor" [GA]) gives

$$M_I = (-7.82 \pm 0.23) \log v_{rot} - 4.43 \pm 0.50 , \quad (4a)$$

with a scatter of $\sigma(M) = 0.63$.

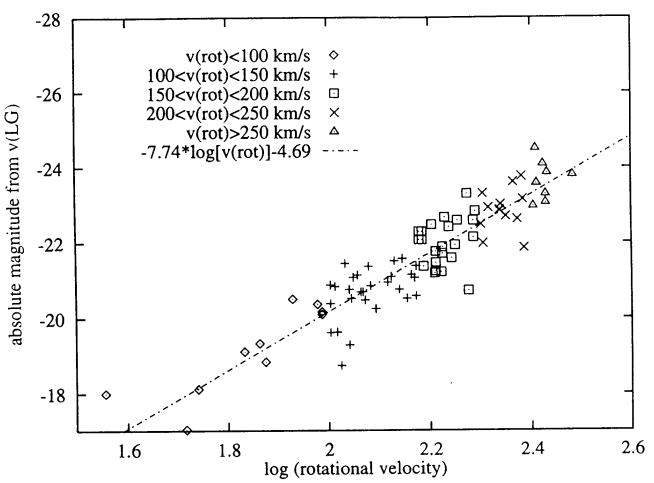

FIG. 7.—Tully-Fisher relation for the 83 galaxies outside the GA direction in the unbiased (i.e., distance-limited) parts of the Spaenhauer configurations of Fig. 5. The total dispersion is $\sigma(M) = 0.59$ mag, but the dispersions of the different rotational velocity bins decrease with increasing rotational velocity. The line is eq. (4b) of the text.

This way of calibrating the slope of the TF relation depends, of course, on the assumption of a linear expansion field. Since the linearity of the expansion in the direction of the putative GA is under discussion (see § 8), we have repeated the determination of the TF slope using only the subsample *away* from the assumed direction of the GA as defined by MFB. The result is

$$M_I = (-7.74 \pm 0.29) \log v_{rot} - 4.69 \pm 0.64 , \quad (4b)$$

with a slightly reduced scatter of $\sigma(M) = 0.59$. We use equation (4b) in what follows.

The brighter subsample, cut at $I = 12.5$ mag, provides the same calibration as equation (4b) within the errors, but the number of galaxies at small rotational velocities is considerably smaller, degrading the accuracy.

Several remarks need to be made.

1. The slope is nearly identical with that adopted by MFB, also said to be unbiased, set out in equation (1) earlier.

2. The slope in equation (4) is different from the slope in equation (2) that applies to the complete sample in Figure 3*a*. The difference is in the direction expected from the bias model of Paper II (Figs. 4 and 7) and in Figure 3*b* of this paper. Because the total sample includes all redshifts, and therefore includes also the flux-limited part of the sample, Figure 3*b* of this paper and Figures 4 and 7 of Paper II show why the slopes of equations (2) and (4) are expected to differ in the way they do. The cause is observational selection bias. The model in Paper II is fully confirmed on this point.

3. Equation (4b) is drawn in Figure 3*a* as a dot-dash line. Besides the slope difference of the line from the main body of the distribution (point 2 above), the most striking feature is the *offset of the line in zero point by* 0.7 mag *from the mean of the main distribution.* This is, of course, the effect of the bias (Fig. 3*b*, and the predictions of the model in Figs. 4 and 7 of Paper II). The 0.7 mag size of this offset is close to what is predicted from the classical Malmquist difference between M_0 (the unbiased apex value) and $M(m)$, where $M_0 - M(m) = 1.39\ \sigma(M)^2 = 0.7$ mag if $\sigma(M) = 0.7$ mag, which we have previously argued (Paper II, § 2.2) to be close to the true value of the intrinsic dispersion.

4. Concerning the last point, the mean dispersion of the unbiased Tully-Fisher relation for the field galaxies in Figure 7 is $\sigma(M) = 0.63$ mag. The dispersion is higher for galaxies with low rotational velocities than for fast rotators. Note that this average dispersion from Figure 7 for the unbiased sample is similar to the dispersions for the different rotational velocity bins in Figures 5 and 6. For the reasons discussed earlier in § 4.1, we believe that these dispersions are not due to peculiar motions but are real.

5. The constant term in equations (4a) and (4b) depends on our arbitrary choice of $H_0 = 50$.

6. INDIVIDUAL CORRECTIONS FOR GALAXIES IN THE BIASED REGION OF THE SPAENHAUER DIAGRAM

The bias-free absolute magnitudes that must be used to compensate for the cutting away of the faint end of the luminosity function by the apparent magnitude limit of the catalog can be calculated either numerically or analytically. The method is to

determine, at each redshift, that absolute magnitude which divides the populated area under the truncated luminosity function into two equal parts. For redshifts less than $v_{\rm limit}$, the absolute magnitude is simply the apex absolute magnitude, M_0(LW), of the particular Spaenhauer configuration. For redshifts larger than $v_{\rm limit}$, where the flux limitation line cuts into the luminosity function, the appropriate absolute magnitude is, of course, brighter than M_0 (apex).

The results of the calculations are shown in the Spaenhauer diagrams of Figures 5 and 6 by the curves threading the individual configurations in the permitted areas. Two lines are shown, one from the analytical calculation similar to that made in Paper II (Fig. 5 and Table 1) and the other from the numerical calculation from the data themselves. Note the general excellent agreement between the analytical and the practical calculation.[4]

The proper bias-free absolute magnitudes derived in this way, both for the $I = 12.5$ mag ("bright") and the "total" MFB sample, are shown explicitly in Figures 8*a* and 8*b* in a different representation than in Figures 5 and 6. The difference in the shapes of the correction curves between the $I = 12.5$ mag and the complete samples are important, teaching the lesson set out in footnote 4 concerning the effect of certain nonrigorous selection criteria used for the "total" MFB sample. These effects, evidently, cause peculiar distributions in the biased areas of these individual SD diagrams, and therefore peculiar correction curves. Note particularly that the shapes of the curves in Figure 8*a* are similar to the expectations from an ideal model (Paper II, Fig. 5), while the curves in Figure 8*b* are not.

We close this section by noting again that the correction procedure set out here is fundamentally different from the Malmquist "global" bias correction, $M_0 - M(m)$. Malmquist's (1920) classical calculation gives, for idealized conditions, the difference in absolute magnitude, *averaged over all redshifts*, between the true absolute magnitude, M_0, which applies to a distance-limited sample, and the mean absolute magnitude, $M(m)$, which applies to a complete flux-limited sample with apparent magnitude cutoff m_c. Contrary to that, we need, and show in Figures 8*a* and 8*b*, the results of a method that gives the individual selection bias corrections for *each redshift* and for *each line width*, based on numerical calculations from the data themselves. These are not formal analytical procedures based on unrealistic samples, but are "self-revealing" corrections based on the properties of real samples.

7. THE HUBBLE CONSTANT AS A FUNCTION OF DISTANCE AFTER APPLYING THE INDIVIDUAL CORRECTIONS

7.1. *The Data as Corrected*

We now return to the initial example in § 3 where we obtained the unphysical result that the Hubble constant increases outward, and further that it is a function of apparent magnitude and rotational velocity if the TF relation is applied "naively" to a flux-limited sample (cf. Figs. 1 and 2). We claim, and show below, that these contradictory results are the consequence of a missing proper correction for selection bias.

The correction procedure, outlined in the previous section, is now applied to the determination of a bias-free *relative* Hubble constant from the MFB data. As in § 3, individual Hubble ratios, $v_{\rm redshift}/d_i$, were calculated for all galaxies in the MFB sample using the proper absolute magnitudes interpolated in Figure 8*a* or 8*b* (according to the sample) at the appropriate individual redshifts and rotational velocities. The corrections are from the "triple-entry" interpolations between line width, redshift, and apparent magnitude catalog limit in Figures 8*a* and 8*b*. The procedure is equivalent to using equation (4b) to compute the (unbiased) apex absolute magnitude and then *adding the bias corrections as functions of redshift and rotational velocity* (i.e., adding the difference between the *level* parts of Figures 8 for small redshifts and the curves beyond the "break redshift," finely interpolated between the curves). These corrected absolute magnitudes are combined with the I-band

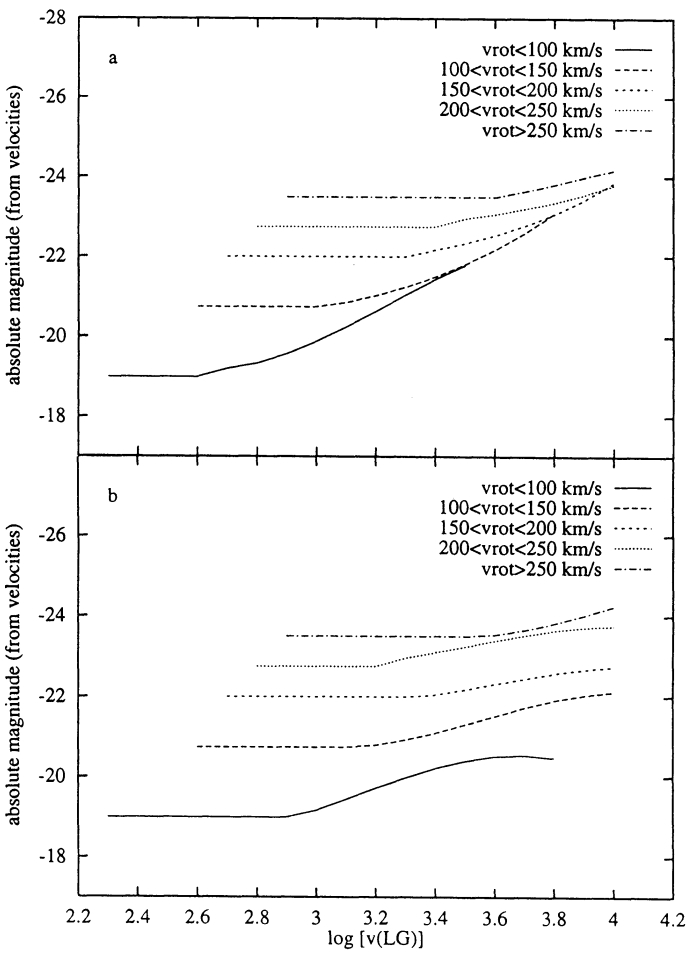

FIG. 8.—(*a*) Derived *proper* absolute magnitudes (*ordinate*) to use at given redshifts (*abscissa*) for given rotational velocities (i.e., LW/2) needed to correct for observational selection bias for the $I < 12.5$ mag ("bright") MFB sample. Absolute magnitudes for each galaxy in the $I < 12.5$ mag subsample have been found by interpolation for each individual rotational velocity and redshift value. (*b*) Same as (*a*), but for the "total" MFB sample.

[4] The *analytical* calculation that generates one of the internal lines in these Spaenhauer diagrams is made under three assumptions: (1) The sample is complete to a well-defined apparent magnitude limit, (2) the luminosity function is Gaussian, and (3) the mean space density for the volume under consideration is constant. On the other hand, the *numerical* calculation that generates the other line is independent of conditions 1 and 2, showing the power of the empirical determination. The method implies, however, condition 3.

The effect of clustering on the calculated mean absolute magnitudes *has* been simulated by Spaenhauer and discussed by Tammann & Sandage (1982, Fig. 2). It is nonnegligible.

It is this effect of nonuniform space density on the *errors* in the bias corrections themselves that makes the search for true peculiar velocity patterns so suspect using any of the known nonredshift distance methods.

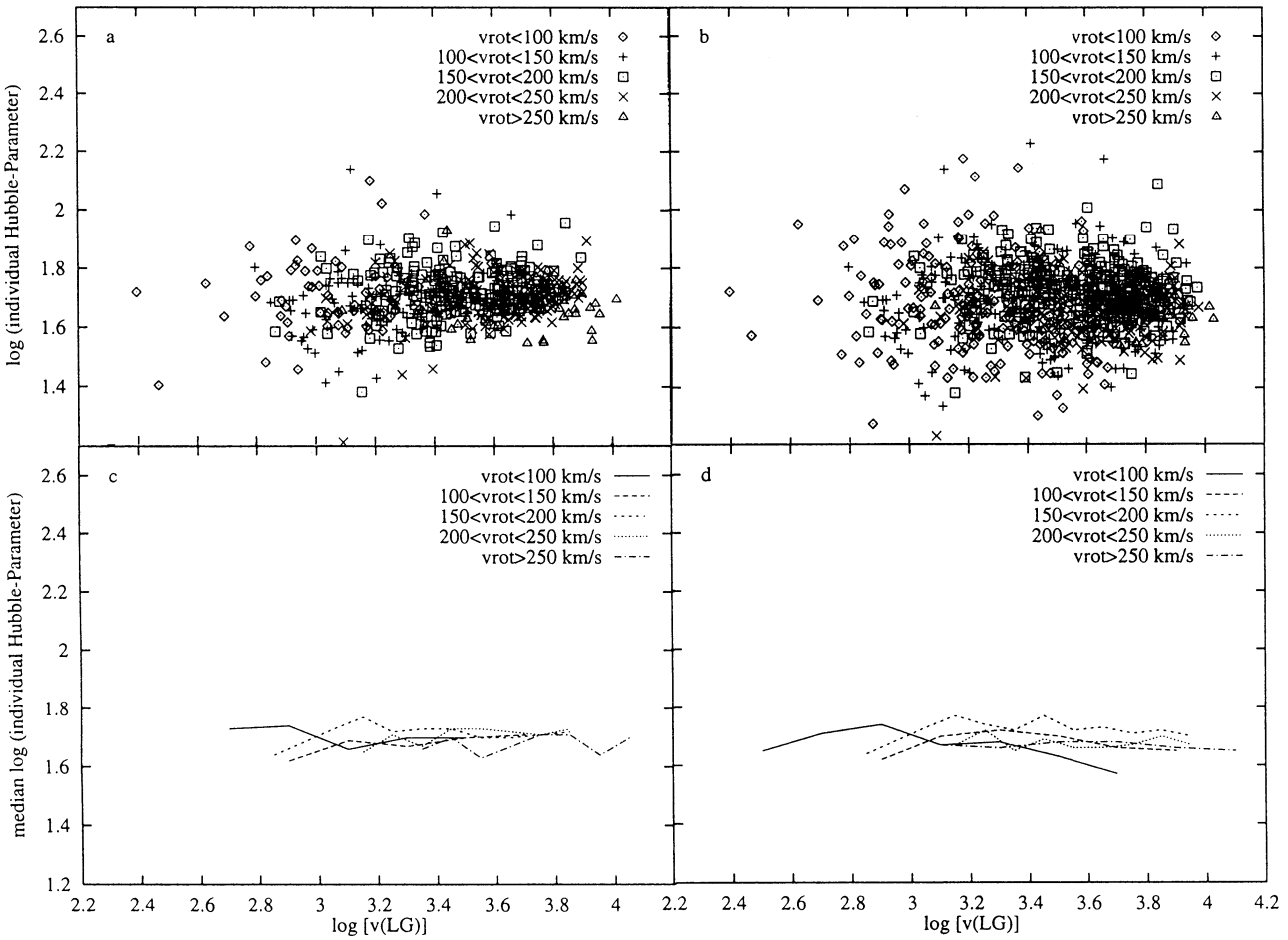

FIG. 9.—Result of applying the Fig. 8 absolute magnitudes as a function of redshift and rotational velocities from Fig. 8*a* to the "bright" MFB sample (panels *a* and *c*) and from Fig. 8*b* to the "total" MFB sample (panels *b*, and *d*). In both cases, galaxies with different rotational velocities give the same mean Hubble ratio at all distances when these corrections are applied. Compare with Figs. 1*c* and 1*d* to see the results of applying these corrections.

magnitudes to give the distance moduli, $(m - M)_I$, that now should contain *no systematic errors with distance, on the average.*

Figure 9 shows the individual Hubble ratios and the mean values, both for the well-defined *bright* sample (Figs. 9*a* and 9*c*, i.e., $I < 12.5$ mag) and for the "total" sample (Figs. 9*b* and 9*d*) of the MFB catalog, after the individual corrections from Figures 8*a* and 8*b* are applied. All systematic effects of the Hubble constant changing with distance have disappeared.

Equally telling is the same point made in Figure 10 compared with Figure 2 in which rotational velocity is the independent variable and redshift is the generator of the family. Of course, Figure 10 is simply Figure 9 in a different representation, no new result being displayed, but the representation is often more satisfying to the intuition.

The following important points need be made concerning Figures 9 and 10:

1. After applying individual corrections to the absolute Tully-Fisher magnitudes, H_0 does not increase outward. At all distances we find the same mean value of the relative Hubble constant within the statistical errors for all rotational velocities and apparent magnitudes.

2. The fact that H_0 is independent of distance for every rotational velocity was forced by the construction on the assumption of a quiet Hubble flow. The premise that permits this construction is that redshift distances are more secure than biased photometric distances. It is this circumstance that provides the possibility for deriving the correction. The fact that the correction procedure works at all (i.e., that the curves in Figs. 9 and 10 are flat) is in favor of the assumption. That the procedure is not flawed by circular reasoning is discussed in Paper II, and in the next subsection.

3. Without the Figure 8 corrections, either the Hubble constant increases outward, or the basic redshift-distance relation is not linear (see Paper I). Neither is correct, from external evidence, meaning that the Fig. 8 corrections must be applied. Both propositions can be disproved by adding a fainter sample and seeing the unphysical properties disappear from the data at the bright level only to reappear again with the same properties at the fainter level. That the bias properties appear and disappear in the way they do (i.e., 0.2 dex in redshift differences for every 1 mag change in absolute magnitude, which the reader can verify by an obvious interpolation in Figures 1, 2, 9, and 10) proves that the apparent effects *are* due to observational selection bias rather than a failure of a linear redshift-distance relation (see § 7.2 below).

4. The intrinsic dispersion of the TF relation that *decreases* with increasing rotational velocity is reflected in Figures 9*a* and 9*b* by the wedge-shaped distribution, tapering to smaller

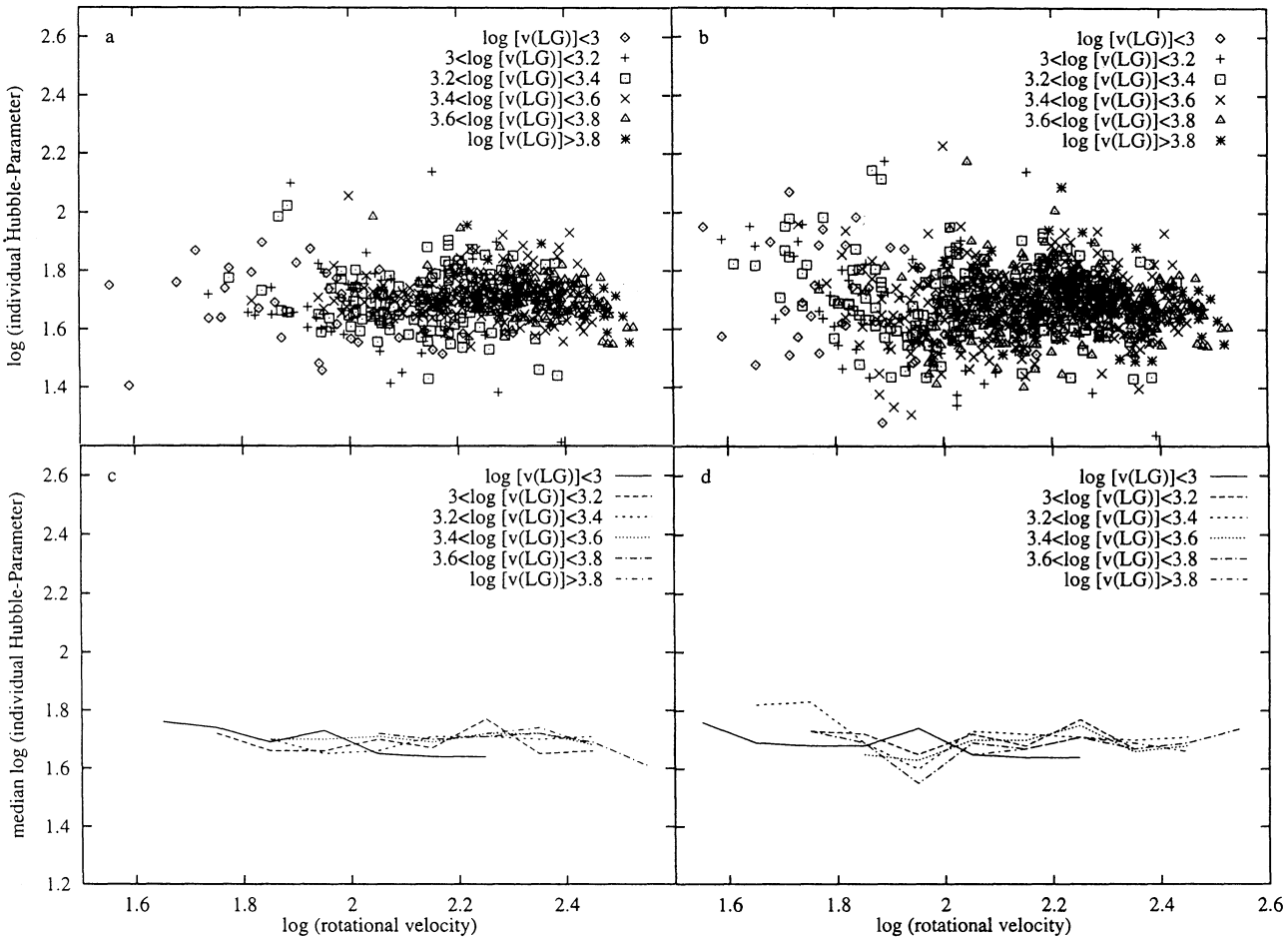

FIG. 10.—Same data as for Fig. 2 for the "bright" sample (panels *a* and *c*) and for the "total" sample (panels *b* and *d*) after the individual corrections for bias have been applied to each galaxy according to Figs. 8*a* and 8*b*. The multivaluedness of the Hubble ratios at a given rotational velocity for different redshifts has been eliminated except for the statistical errors. Compare with Figs. 2*c* and 2*d* for the same data without the Fig. 8 corrections.

total spread at large redshifts. Said differently, the range of Hubble ratios for the smaller, and on average closer, galaxies with low rotational velocities is much larger than for the, on average, more distant and larger galaxies with high rotational velocities. The apparent spread in the individual h_i values in Fig. 9 is, of course, due to the statistical errors in the individual photometric distances resulting from the intrinsic dispersion in the Tully-Fisher relation.

5. Although the family of lines in Figure 9*c* and 9*d* and Figures 10*c* and 10*d* all collapse almost to the same mean value of H at all redshifts (compare with the raw data in Figs. 1*a*, 1*b*, 2*a*, and 2*b*), recovering the *input* value of $H_0 = 50$ (which it must if our procedure is correct), the individual lines do not coincide *exactly* due to poor statistics, shown directly for the slowest rotators ($v_{rot} < 100$ km s^{-1}), where the demonstrated statistical errors are highest.

7.2. *Circularity?*

Critics will argue that we have assumed a linear redshift-distance relation and then derived the corrections in Figures 8*a* and 8*b* to make the initial assumption come about at every redshift and at every line width, simply recovering the input assumption. If the redshift-distance relation locally is in fact nonlinear, then the corrections in Figure 8 are meaningless because they will be said to be nothing more than the requirement to recover the input assumption (which might be wrong).

The disproof of this argument of circularity is as follows. As mentioned often above, the basis of the proof is the effect on the Spaenhauer diagram of adding a fainter sample. The method as originally proposed (Sandage 1988a, b) was to see whether the apparent property of an increase in the absolute luminosity with redshift would disappear near the limit of the bright sample but reappear near the corresponding level of the faint sample at the rate of 1 mag per 0.2 dex in redshift. The procedure was to add objects of the *same intrinsic absolute magnitude but at a fainter apparent magnitude.*

Now, the effect of using Tully-Fisher data is equivalent to considering objects in a catalog with the *same limiting apparent magnitude* but adding galaxies of *fainter absolute magnitudes* to the SDs. This is done automatically in the TF method by analyzing *by line width* and noting that adding different line widths at *fixed* apparent magnitude (as done here is Figs. 1, 2, 5, and 6) is the same as adding a fainter sample in apparent magnitude at fixed absolute magnitude. Consequently, the test is the same, in principal, as originally set out.

The basis of the method was initially tested using three catalogs of Sc I galaxies with different limiting magnitudes ($B = 13$ mag and $B = 15.5$ mag) (Sandage 1988a). A second discussion

using S0 + Sa galaxies, again from two catalogs with different limiting magnitudes, showed the effects (Paper I of this series). The result was that bias was proved rather than that the redshift-distance relation is nonlinear.

But, alternatively, we could simply have used external data from the beginning, taking as known that the expansion field is, in fact, linear[5] to first approximation. This would make moot directly the question of circularity, no further proof of linearity being necessary. The previous evidence to be cited in support of this precept would include the Hubble diagram of clusters and groups (Sandage 1972b, 1975, Figs. 4 and 5; Sandage & Hardy 1973; Sandage & Tammann 1975 [Fig. 6], 1990 [Fig. 1]; Sandage 1992; Tammann 1992; Lauer & Postman 1992; Jerjen & Tammann 1993), the linear decrease of angular diameters of cluster galaxies with increasing redshift (Sandage 1972a), the very local redshift-distance relation determined from Cepheids (Sandage 1986), and the evidence from the Hubble diagram derived from supernovae (Sandage & Tammann 1993). If the argument were to be made in this way by adopting the linearity *as an initial premise*, then (*a*) Figures 1–7, (*b*) the correction diagrams in Figure 8, and (*c*) the corrected diagrams in Figures 9 and 10 and the previous arguments based upon them would follow directly with no circularity.

8. THE LOCAL AND NOT SO LOCAL EXPANSION FIELD

The results of the preceding section can be illustrated in an alternative way which also reveals information about the local expansion field. We inquire first into the nature of the Hubble diagram (redshift versus photometric distance) using TF distances, both uncorrected and corrected for bias to see the difference.

8.1. *The Hubble Diagram with and without Bias Corrections*

Figure 11*a* (note the log-log axes) shows the redshift-distance relation for the complete MFB sample using the "unbiased" TF relation (eq. [4b] from Fig. 7), to calculate photometric distances *but no corrections* are applied for selection bias to the distances of individual galaxies (i.e., we use only *apex* absolute magnitudes, M_0(LW), not the bias-corrected absolute magnitudes from Fig. 8*b*). The redshifts in this and the following three diagrams (Figs. 12–14) are reduced to the centroid of the Local Group, denoted as v(LG). The two lines are for Hubble constants of 50 and 100, respectively.

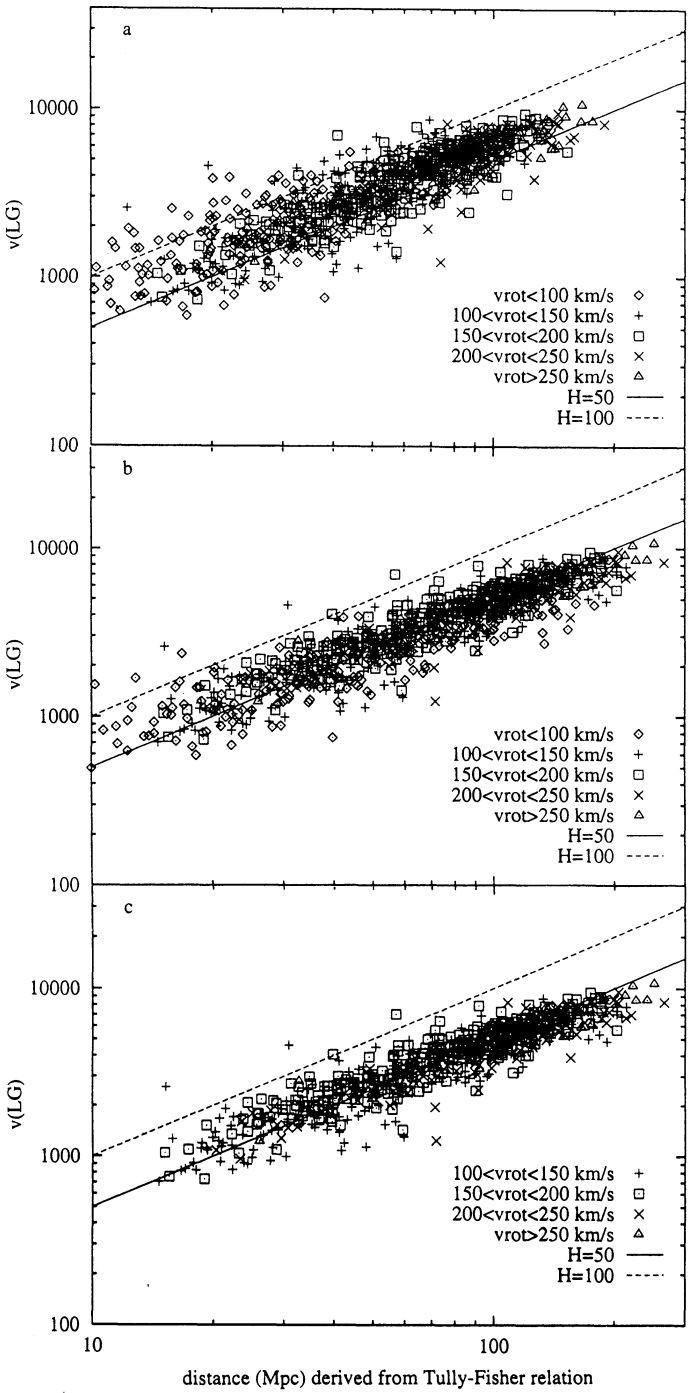

FIG. 11.—Hubble diagrams (log-log axes) for galaxies in the MFB "*total*" sample stacked according to rotational velocity using different symbols. The redshifts, v(LG), are referred to the kinematic frame of the Local Group. The effects of bias corrections on the apparent value of H_0 are shown in the three panels. A contradiction exists if these diagrams do not recover the *input* value of $H_0 = 50$. Lines for H_0 of 50 and 100 are shown. (*a*) Data without individual correction for selection bias. The mean value of H_0 is ~ 70, whereas the input value is $H_0 = 50$. This is the same contradiction, but in a different form, as shown by the offset between the data and the mean line in Fig. 3*a*. (*b*) Same galaxies as in (*a*), but using the individual absolute magnitudes in Fig. 8*b*, i.e., as corrected for observational selection bias. (*c*) Same as (*b*), but excluding the data of the lowest rotational velocity bin. H_0 is generally 50 except at the lowest redshifts. The deviation from linearity here is due to problems with the sample as proved by Fig. 12.

[5] Throughout this paper we have assumed a strictly linear expansion, no account being taken of peculiar or streaming motions. It is to this level of approximation that the bias corrections have been determined in Fig. 8. The statistical distances we derive are then good only to the accuracy of this approximation.

Linearity of the global expansion field is beyond doubt, first shown by Hubble & Humason (1931), and more recently in a series of papers, of which those by Sandage & Hardy (1973) and Kristian, Sandage, & Westphal (1978) give references.

However, the assumption of strict linearity in all directions of the local sky in not entirely obeyed, seen by the uncontested existence of the CMB dipole signal showing that (1) the local velocity field is perturbed and therefore (2) that noncosmological motions exist, small as they may be on a global scale.

It is, of course, the hope that even the first-order bias corrections derived here are good enough at some level to reveal even smaller peculiar and streaming motions than the CMB dipole. This hope may be realized as a shadow in the discussion in § 8, but the time for a full discussion of the deviations apparently seen in Figs. 15*b* and 15*d* below does not seem quite ripe for us yet. We are concerned in this paper only with the first-order corrections to the statistical distances and the effect on the determination of the global (Machian) value of H_0.

The astonishing feature, and *the major contradiction*, in Figure 11*a* is that the mean (output) Hubble constant for the entire sample is near $H_0 = 70$. This is a contradiction because equation (4b) is based on the arbitrary relative scale of $H_0 = 50$ as input. Hence, the naive application of the TF relation to calculate distances (without bias corrections) *does not recover the input value* of H_0, demonstrating directly the effects of bias.[6]

The problem is partially solved in Figure 11*b*, which shows the result of applying the Figure 8*b* absolute magnitudes to the total sample, interpolated in redshift and rotational velocity for each individual galaxy, i.e., correcting the sample for selection bias. The bulk of the data beyond 2000 km s^{-1} (40 Mpc) now *follow the* $H_0 = 50$ *line, recovering the input value of* H_0. However, the scatter in Figure 11*b* is large, caused primarily by the large intrinsic dispersion of the slow rotators with $v_{rot} <$ 100 km s^{-1}. These are eliminated in Figure 11*c*, appreciably reducing the scatter.

However, the remaining problem with Figure 11*c* is the nonlinear character of the diagram for all redshifts in the surveyed range. The correlation has a tilt over the entire distance range, showing an apparent *decrease* in the effective Hubble constant outward, imitating a nonlinear redshift-distance relation in the *opposite* sense claimed by Tully (1988) and others previously cited. We first suspected that this could be removed by changing the slope of the TF relation in equation (4b). However, extensive numerical experiments using even extreme slope coefficients proved that the nonlinear effect in Figure 11 *could not* be removed in this way. We then suspected that the apparent deviation is due to the heterogeneous nature of the total MFB sample (again excluding clusters) caused by the method of selection (see footnote 4). To test this, we repeat Figures 11*a*, 11*b*, and 11*c* in Figure 12 using only the more homogeneous $I < 12.5$ mag sample. We further use only that part of the sample away from the direction of the putative GA (see Dressler & Faber 1990a, b) because our immediate purpose is simply to demonstrate the effects of bias with and without correction rather than to test for linearity, which has been well proved before by independent means.

Figure 12*a* is the same as Figure 11*a*, but for the $I < 12.5$ mag sample and in the anti-GA direction, using only equation (4b) (i.e., *without* individual bias corrections). Figure 12*a*, like Figure 11*a*, shows an average Hubble constant of $H_0 = 70$, failing to recover the input assumption of $H_0 = 50$. Again, naive application of TF gives the wrong answer grossly, *giving too high a value* for H_0.

Figure 12*b* uses the individual absolute magnitudes from Figure 8*a*, i.e., corrected for selection bias and again only using galaxies in the anti-GA direction. The mean Hubble constant is now close to $H_0 = 50$, as it must be if the method works (i.e., again the output H_0 must recover the input value). But again the scatter is high as in Figure 11*b*. The scatter is reduced in Figure 12*c* by eliminating the slow rotators from Figure 12*b*.

Now, *the redshift anomaly in Figure 11 for* $v(\mathrm{LG}) < 2000$ km s^{-1} *is also largely removed.* All points at all redshifts define nearly the same mean H_0 line in Figure 12*c*. Hence, the more ideally selected $I < 12.5$ mag sample gives textbook results, illustrating the effect of the observational selection bias. In the

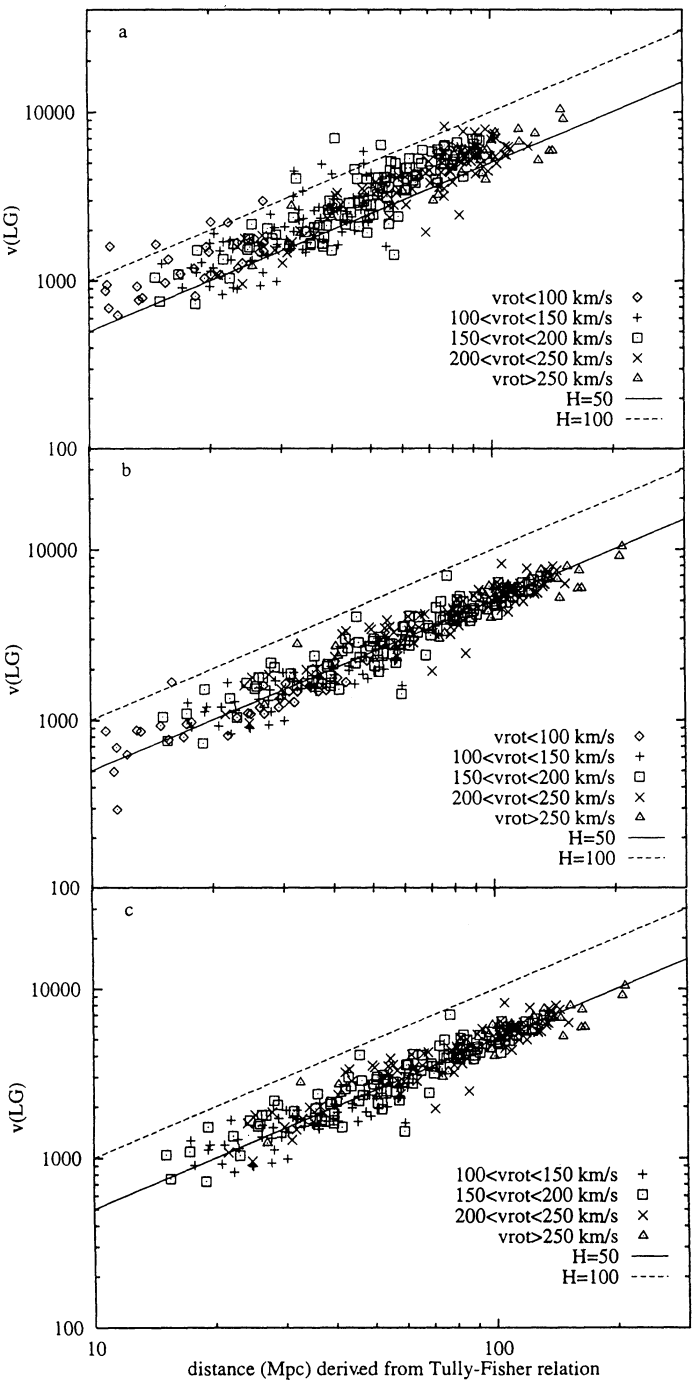

FIG. 12.—Same as Fig. 11, but for the "*bright*" subsample with $I < 12.5$ mag and in a direction away from the putative Great Attractor: (*a*) without individual bias corrections; (*b*) for the same galaxies as in (*a*), but with the bias corrections of Fig. 8*a* applied; (*c*) the same as (*b*), but without the slowest rotators. The linearity of the redshift-distance relation at small redshifts has been restored in (*b*) and (*c*) by these restrictions to a "proper sample."

[6] This in a more subtle form (subtle because the data are from "clusters" and "groups," and the bias properties, although also present, are, nevertheless, different) is, of course the case of an incorrect conclusion that H_0 is high (cf. Pierce & Tully 1992; Mould et al. 1993) when using local calibrators. These calibrators are valid for a strictly *distance-limited* sample, whereas the data to be analyzed are not. A distinction must be made between a distance-limited sample and a sample (complete or incomplete) where all objects are at the same distance. There is selection bias in the latter, explaining why all the results giving a high value of H_0 using clusters and groups are suspect using incomplete samples with no bias corrections.

remaining sections, any conclusions from the fainter "total" sample should clearly be given lower weight.

Said specifically, to remove the slope problem in Figure 11*c*, it is more important to use the magnitude-limited subsample ($I < 12.5$ mag) than to use only anti-GA galaxies in the MFB data base. Nevertheless, the total problem in Figure 11*c* can only be removed by the double restriction of using only the $I < 12.5$ mag sample and using only galaxies outside the GA direction whose rotational velocities are greater than 100 km s^{-1}. With this restricted sample, the redshift-distance correlation in Figure 12*c* is seen to be ideally linear.

8.2. *The Linearity of the Very Local Expansion Field*

Having shown the power of the individual bias corrections in the various comparisons in both Figures 11 and 12, we now comment on the local velocity field using, in turn, the "total" MFB sample and the strictly selected $I < 12.5$ mag subsample in different directions.

Figure 13*a* shows the Hubble diagram (with linear axes for both redshift and distance) for the "total" MFB sample that is in the region *away* from the GA as defined by MFB. The distances are calculated using the absolute magnitudes from Figure 8*b*, individually applied to each galaxy by interpolation for each particular redshift and rotational velocity value. The redshifts are relative to the kinematic frame of the Local Group.

The scatter increases in a opening wedge pattern for larger distances, as expected if the scatter is due to the intrinsic luminosity spread given by the luminosity function rather than the result of a spread in redshift due to peculiar motions. Clearly, any spread in redshift due to peculiar motions is small compared with the overwhelming spread in absolute magnitude (see Fig. 19*c* below). This is the argument made often before (e.g., Sandage & Tammann 1975) and is a strong diagnostic for a spread in absolute magnitude but not for residual velocities about a quiet Hubble flow.

The two lines in Figure 13*a* are for Hubble constants of $H_0 = 50$ and $H_0 = 100$. (Note again that the arbitrary *input* H_0 is 50, upon which Fig. 8 is based). The most distant galaxies (i.e., $d > 150$ Mpc; $v > 7500$ km s^{-1}) seem to require a systematically lower value of H_0. We believe this to be unreal because our distance scale here is so sensitive to the exact value of our bias corrections in Figure 8 at large redshifts. Only very small changes in these corrections are required to remove the apparent nonlinearity. For what follows, we stress that distances greater than 150 Mpc ($v > 7500$ km s^{-1}) should, consequently, be given little weight.

Figure 13*b* is the Hubble diagram for the direction *toward* the GA using the "total" sample, and using the individual absolute magnitudes to correct for bias interpolating in Figure 8*b*. The diagram is slightly noisier than Figure 13*a*, which contains only galaxies away from the GA. In addition, the nearer galaxies in Figure 13*b* appear to lie above the H_0 line, whereas the most distant galaxies lie below as in Figure 13*a*. The clumpiness and the systematics of the deviations from an ideal Hubble flow in the distribution in Figure 13*b* are due, we believe, to the clumpy nature of the space distribution in this direction. The sight lines traverse the well-known groups in Hydra, Centaurus, Antlia, Dorado, etc. This region of the sky is very noisy in its spatial nonuniformity (de Vaucouleurs 1975; Sandage 1978), and therefore, by implication, in the larger than usual velocity perturbations that are expected about the underlying global cosmological expansion.

The data for the more ideal subsample of the MFB catalog, i.e., cut strictly at $I = 12.5$ mag, are shown in Figure 14*a* away from the GA and in Figure 14*b* in its direction. *No systematic deviations from linear expansion are present in Figure 14a.* The expansion in the GA direction (Fig. 14*b*) also appears linear, except for the nearer galaxies within $r < 50$ Mpc ($v < 2500$ km s^{-1}). These galaxies show a systematically higher local value of H_0, but only in this restricted (and noisy) direction. Again, note the lack of a velocity perturbation in Figure 14*a* in a direction nearly at right angles. Note also the fact that we recover the input value of H_0 after applying the mean bias corrections from Figure 8*a*.

The redshifts v(LG) have been transformed into v(220) velocities in Figure 15, i.e., corrected for the gravitational pull of the Virgo Cluster and its halo. The necessary velocity correc-

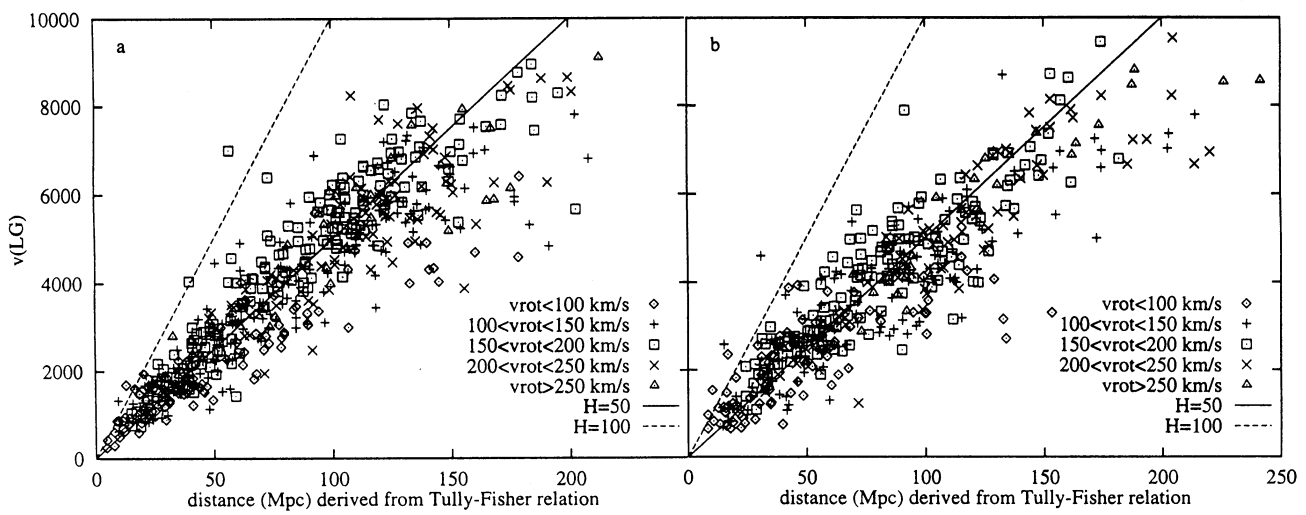

FIG. 13.—Hubble diagrams (linear axes) for the "total" MFB sample. The velocities, v(LG), are referred to the kinematic frame of the Local Group. The two lines define H_0 values of 50 and 100. The input value of $H_0 = 50$ must be recovered if the bias corrections herein are valid. (*a*) Galaxies in a direction away from the apex of the "Great Attractor." (*b*) Galaxies in the direction of the "Great Attractor."

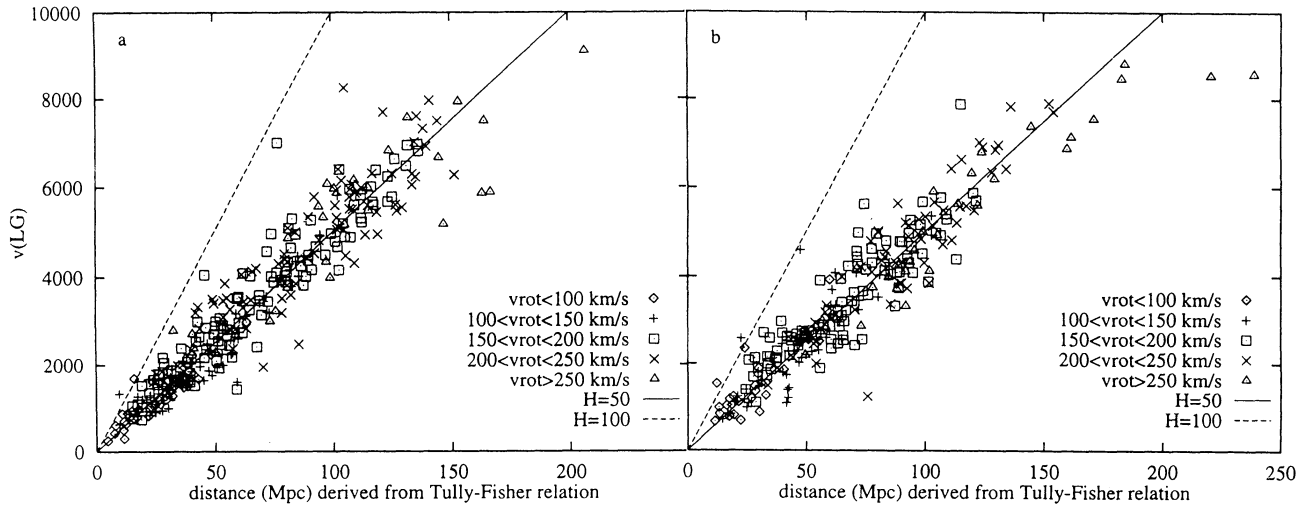

FIG. 14.—Same as Fig. 13, but for the "bright" MFB sample away and toward the directions of the GA in (*a*) and (*b*), respectively. The input value of $H_0 = 50$ is recovered, showing the consistency of the bias corrections.

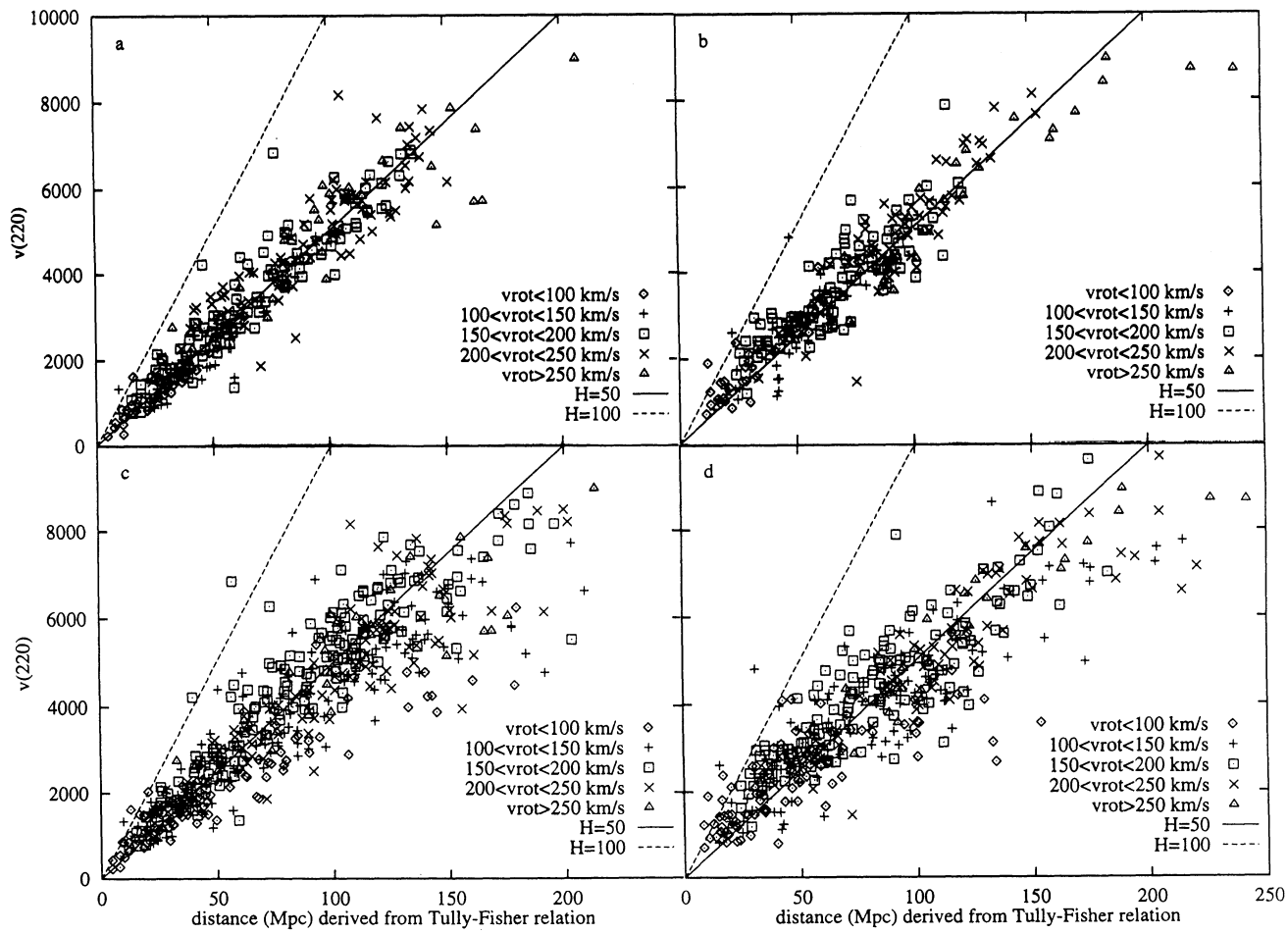

FIG. 15.—Same as Figs. 13 and 14, except the redshifts are referred to the kinematic frame of the Local Supercluster centered on the Virgo complex. The method of obtaining the $v(220)$ values is explained in the text. Panels *a* and *b* are for the "bright" sample, (*a*) with galaxies away from the GA and (*b*) with galaxies toward the GA. Panels *c* and *d* are for the "total" sample, (*c*) with no galaxies toward the GA, and (*d*) with galaxies in the direction of the GA. Galaxies in (*b*) and (*d*) have excess velocities over the mean Hubble line for line for $H_0 = 50$ for $r < 60$ Mpc. The effect here is clearer than in Figs. 13*b* and 14*b* (see text).

tions, $\Delta v(220)$, are calculated following the model of Kraan-Korteweg (1986a, b) using an "infall" (actually a retarded expansion rate) Virgocentric velocity vector of 220 km s^{-1}.

The Hubble diagram using the resulting $v(220)$ values and the unbiased TF distances is shown in Figures 15*a* and 15*c* for the "bright" and "total" samples, respectively, for the region outside the GA. Comparison with the corresponding Figure 14*a* shows a slightly reduced scatter here, consistent with the reality of a Virgocentric "infall." Figures 15*b* and 15*d* are again for the "bright" and the "total" samples in the direction of the GA.

Note the signal for a velocity *excess* for the galaxies with $r < 50$ Mpc ($v < 2500$ km s^{-1}) *in the direction* of the GA. This is seen by the elevation of the points at a distance of 40 Mpc in Figures 15*b* and 15*d*. The signal here is even stronger than in Figure 14*b*. Many of the nearer galaxies in this restricted direction appear to be falling *away* from us, having individual Hubble ratios, h_i, of 70–80 km s^{-1} Mpc^{-1}.

We believe this feature to be real, not a product of an inaccurate bias correction (note its *absence* in Figs. 14*a* and 15*a*, where the same bias corrections have been applied). It is evidently a part of the complex flow pattern in this direction, superposed on the underlying cosmological true linear expansion, as discussed in § 8.3 and hinted at in footnote 5. The anomaly will be discussed in a later paper pending more data, but we stress that none of the ~20 galaxies that show the velocity excess have $v(220) > 3000$ km s^{-1}, and hence the data here *have no relation with the GA at* ~4500 km s^{-1} (Dressler & Faber 1990a, b, hereafter DF; Burstein, Faber, & Dressler 1990).

8.3. *The Local* "500 km s^{-1} *Offset*" *in the CMB Frame*

Figures 16*a* and 16*b* show the Hubble diagrams for the "bright" $I < 12.5$ mag sample *toward* and *outside* the direction of the dipole of the cosmic microwave background (CMB) whose apex is at Galactic coordinates $l = 277°$, $b = +30°$. The results are relative to the kinematic frame of the CMB calculated by subtracting a simple dipole motion of 630 cos A km s^{-1} from each galaxy, where A is the angle from the apex of the CMB dipole to the galaxy in question. While the plot in Figure

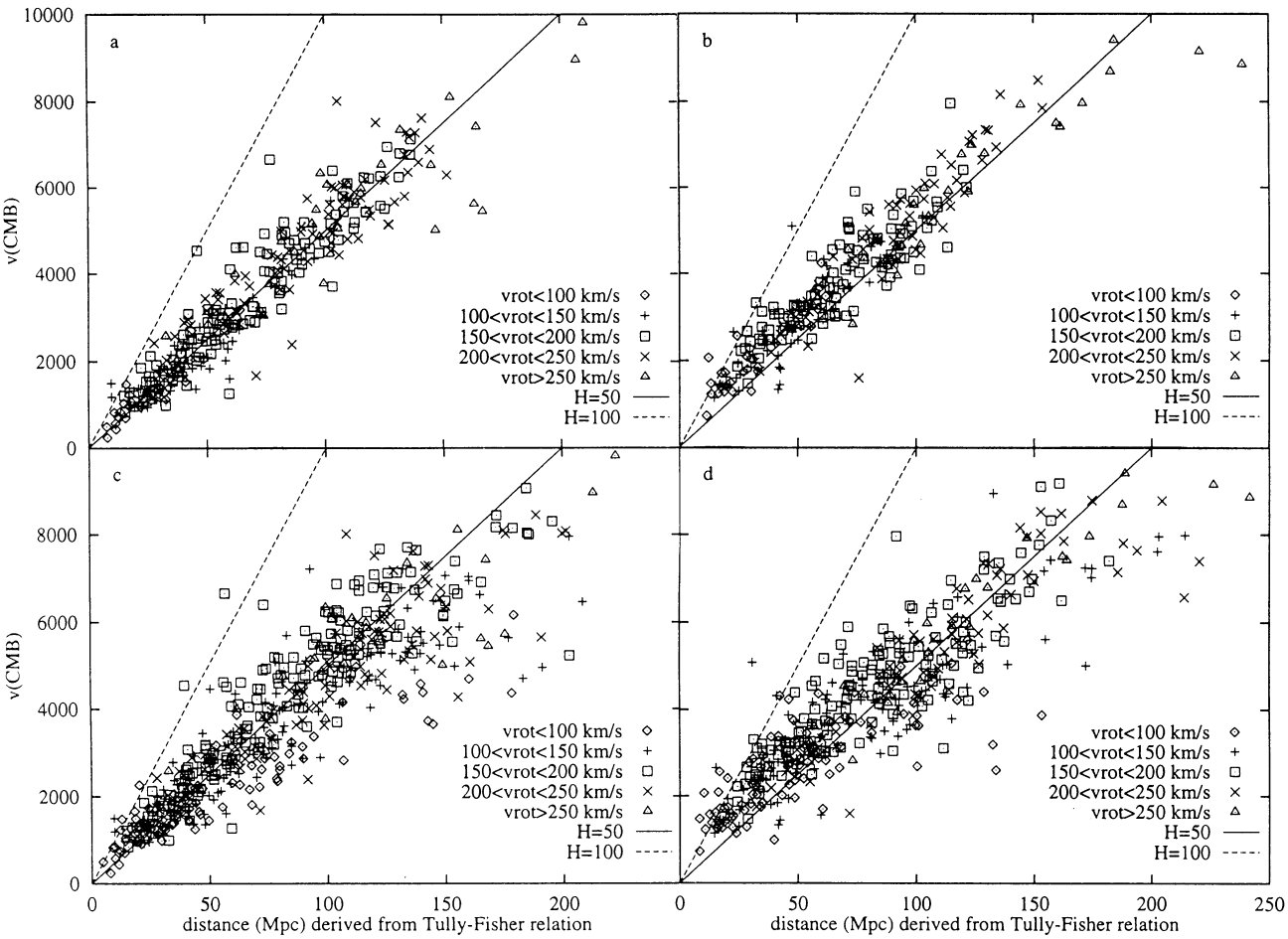

FIG. 16.—Hubble diagrams similar to Figs. 14 and 15 for the "bright" ($I < 12.5$ mag) sample, with (*a*) and (*b*) outside and within the GA direction, respectively, and the "total" sample, with (*c*) and (*d*) separated as in (*a*) and (*b*) relative to the GA, but with the redshifts *referred to the kinematic frame of the CMB*. The 500 km s^{-1} offset found by DF and by MFB is present in (*b*) and (*d*) for the direction of the GA but is not present in (*a*) for the direction outside the GA. The nearer galaxies ($r < 70$ Mpc) in the direction of the GA, (*b*) and (*d*), have a clear excess velocity of ~500 km s^{-1} above the H_0 expansion line in the CMB kinematic frame. If this offset were distance-independent, it would require a *coherent* bulk motion, roughly in the direction of the GA. However, the excess velocity *approaches zero* near $r \sim 80$ Mpc, and therefore *has a radial gradient* (see Figs. 17*b* and 17*d*). This requires an *incoherent* local motion, *dying out* with increasing distance. Therefore, it is not a bulk motion in detail over its entire range.

16*a* outside the GA remains nearly unchanged[7] from Figure 15*a*, the region toward the GA in Figure 16*b* now shows a clear offset of ~ 500 km s^{-1} for the nearer galaxies not seen in Figure 15*a*. The offset has been pointed out before by Mathewson, Ford, & Buchhorn (1992a, b) and was discovered independently by DF from other data.

The interpretation of the offset is obvious. If the dipole of the CMB is due to a peculiar motion at all, it must show as an offset from the Hubble line in Figure 16*b* for those galaxies that partake in this motion. In other words, the Local Group moving together with some comoving bubble of unknown (at this point in the argument) size *must* reveal a streaming motion relative to the Machian frame *set by the CMB*. Figure 16*b* shows that the nearer part of the MFB sample is indeed not stationary in the comoving CMB frame but rather is stationary (to first order) in the frame of the *Local Group* (i.e., in Fig. 14*b*). Said differently, comparing Figure 14*b* with Figure 16*b* shows that *the Local Group and the nearer part of the MFB sample are moving more or less together as a local bubble* (but one which has within it shear and radial gradients of the streaming amplitude) as in the earliest discussions of the motions relative to the CMB (Shaya 1984; Sandage & Tammann 1984; Tammann & Sandage 1985).

DF have interpreted the "500 km s^{-1} offset" (Fig. 16*b*) (actually the value is 650 ± 30 km s^{-1} as determined to better advantage in Figs. 17*d* and 18*d* below) in the CMB apex direction differently. They have assumed an infall *into a single attractor*, i.e., the GA at 4000–4500 km s^{-1} toward $l = 309°$, $b = 18°$. However, existing models of the GA by Burstein et al. (1990, hereafter BFD) predict the flow velocities to *increase* up to a streaming velocity superposed on the Hubble flow of $\Delta v_{\text{streaming}} \sim 1000$ km s^{-1} as one approaches the GA, whereas the data here for the perturbation about the cosmological flow in fact *decrease* with increasing distance from us (cf. § 8.4 and Fig. 17*b* below), eventually going to zero at about $v \sim 4500$ km s^{-1}, just at the redshift where the perturbation should be a *maximum* on the Great Attractor model.

Moreover, the BFD model also predicts a *backside* infall into the GA. The predicted BFD infall pattern for galaxies in an annulus of 10°–20° radius about the GA is shown in Figure 17*b* by the S-shaped curve. The observations here are at variance with this model for distances larger than ~ 70 Mpc, and they certainly deny the back-side infall predicted by the model.[8]

We thus agree with MFB that this predicted back-side infall at 4000 km s^{-1} is denied by the data. It appears rather that both the 500 km s^{-1} offset and our motion toward the CMB apex are the result of a peculiar velocity vector caused by *several* galaxy clusterings which act as accelerators (Kraan-Korteweg, in a diagram shown by Tammann & Sandage 1985, Fig. 5) *within* the 4000 km s^{-1} "bubble."

But we also disagree with Mathewson et al. (1992b), and consequently also with the similar later claim of Lauer & Postman (1992), where both state that the comoving bubble (moving in bulk flow according to them) has a coherence length of more than 13,000 km s^{-1}. Distances to field galaxies are not presently well enough determined to permit detection of a 500 km s^{-1} signal at this large distance. This requires an accuracy $\Delta v/v = \Delta r/r$ of 500/13,000 = 4%, which is beyond all present accuracies for photometric distances.

How large then, in fact, is the "local bubble" (or supercluster) that is falling toward the Hydra apex with a velocity of 495 km s^{-1}? (The apex direction and the velocity amplitude are given by the vector difference between the observed CMB dipole and our infall to Virgo; Tammann & Sandage 1985, Fig. 3.) To answer, we plot the data from Figure 16 in Figures 17 and 18 as velocity residuals, obtained by subtracting the *observed* redshifts, corrected to the CMB kinematic frame, *from the pseudocosmological redshift*, i.e., 50*r*(TF) (i.e., as if our unbiased TF distance are correct). Median lines (using 10 Mpc bins) through the points are shown in Figure 17.

In the direction outside the GA (Fig. 17*a*) the median line is virtually flat. However, toward the GA (Fig. 17*b*) the ~ 500 km s^{-1} offset is *starkly evident*, and, as emphasized previously, with an amplitude that decreases, rather than increasing, with distance from us. This is not the signal of a Great Attractor, for the reasons just discussed.

Because we believe that the "500 km s^{-1} offset" so evident in Figures 16*b*, 16*d*, 17*b*, 17*d*, and 18*d* is the *same motion that causes the CMB dipole*, it is physically more meaningful to separate the data in Figure 17 into a region within 45° of the warm CMB pole and a region outside this direction, rather than separating the galaxies depending on their position relative to the GA (as in Fig. 17), which is some 30° away. The data separated in this way are shown in Figure 18. Figure 18*a*, for data *outside* the CMB apex direction, is nearly the same as Figure 17*a*.

Figure 18*b* shows the velocity offset due to the dipole motion toward the warm CMB pole. Read from Figure 18*b*, this local velocity perturbation, clearly the same as in Figure 17*b* and *d*, again decreases toward zero with distance, but the statistical variations are yet too large, using the small sample, to determine with any confidence the "precise" distance where it becomes zero. Nevertheless, the data are good enough to show again that distance is surely less than 13,000 km s^{-1} (260 Mpc) determined both by MFB and by Lauer & Postman (1992). An adjudication of these contrary results is a problem for the future in the next step in an analysis of this "local" perturbation on an ideal cosmological expansion redshift.

However, as in Figure 17*d* using the "total" sample with redshifts referred to the GA direction (which is nearly the same as the CMB for this purpose), the distance at which the perturbation dies must be at roughly 4000–4500 km s^{-1} (80–90 Mpc).

Clusters of galaxies also show that the scale for the "local bubble" is less than 6500 km s^{-1} (Jerjen & Tammann 1993), while recent results from *IRAS* galaxies give 3500–4000 km s^{-1} (Lynden-Bell, Lahav, & Burstein 1989; Strauss et al. 1992). These estimates are consistent with one another but are a factor of ~ 3 smaller than stated by Mathewson et al. (1992b) and Lauer & Postman (1992) at $v > 13{,}000$ km s^{-1}.

8.4. *The Problem of Detecting Peculiar Motions*

The only method of detecting peculiar motions superposed on a quiet Hubble flow is to read the Hubble diagrams of Figures 13–16 vertically as velocity residuals and to search for systematics in them that can be separated from the overwhelming signal due to the errors in the distance caused by the intrinsic dispersion of the absolute magnitudes.

[7] The reason why no velocity offset is present in Fig. 16*a* is that most of these galaxies "outside the GA region" are nearly at right angles to the apex of the CMB direction. The "correction to the CMB frame" is then very small.

[8] With a bit of fantasy one could see the signal of a back-side infall in the "total" sample in Fig. 17*d*. However, it comes at a distance where our bias-corrected distances become unreliable, seen directly by a comparison with the data *outside* the direction of the GA in Fig. 17*c*.

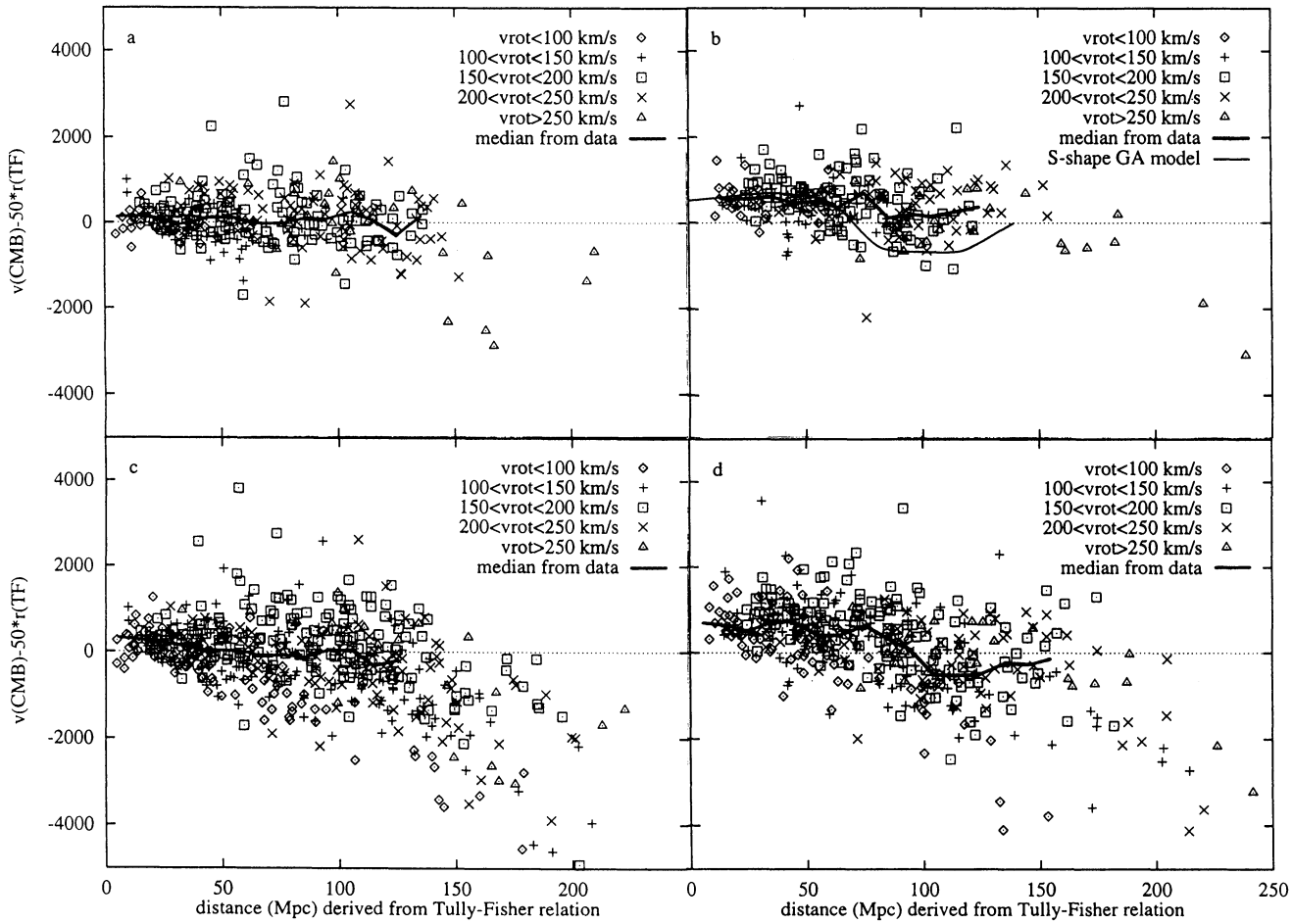

FIG. 17.—Velocity residuals as a function of distance ($H_0 = 50$) for galaxies in Fig. 16. (*a*, *c*) Outside the GA. The median line drawn through the points agrees well with the expectations of zero deviations from an ideal linear cosmological expansion except for the most distant and hence most uncertain points. (*b*, *d*) In the direction of the GA. The median line through the points shows a clear excess velocity of 650 ± 30 km s^{-1}. The excess velocity approaches zero gradually, reaching it at ~80–90 Mpc ($v \sim 4000$–4500 km s^{-1}). Panels *a* and *b* are for the "bright" sample; panels *c* and *d*, for the "total" sample. The S-shaped (*lower*) curve in (*b*) is the *predicted* front-to-back infall in the model by Burstein, Faber, & Dressler (1990) if the putative GA had a gravitational effect on the expansion field. The curve does not fit the data for distances greater than 70 Mpc; it has too large an amplitude relative to the data that show no evidence for a back-side effect.

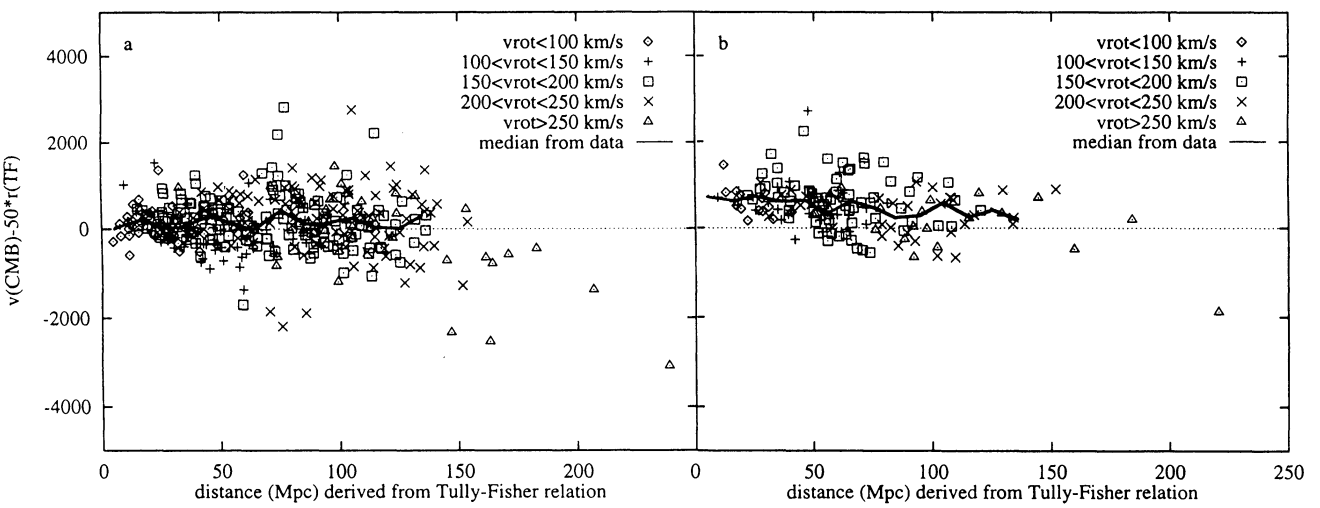

FIG. 18.—Same as Fig. 17, showing residuals read as velocity differences for the "bright" sample, but now referred to directions associated with the position of the dipole of the CMB radiation rather than directions associated with the putative GA. (*a*) Directions away from the CMB pole and antipole with angles greater than 45° from either. Note the near-zero offset in the mean. (*b*) Closer than 45° from the direction of the pole showing a CMB dipole velocity offset of 650 ± 30 km s^{-1}.

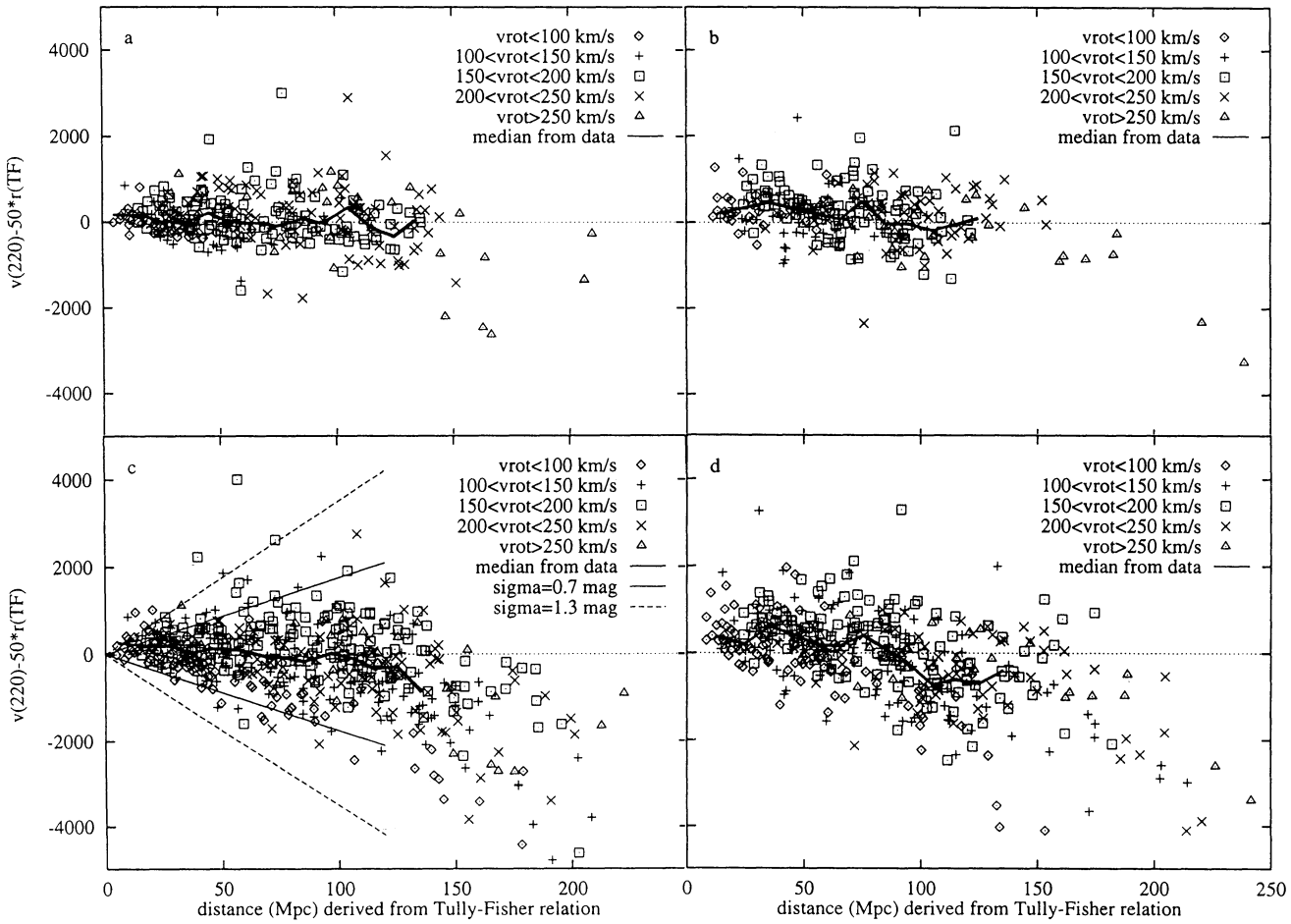

FIG. 19.—(*a*, *b*) Same as Fig. 17, but with the redshifts referred to the kinematic frame of the Virgo Cluster and in a direction *away* from the putative GA. Panel *a* is for the "bright" sample, showing no velocity offset; panel *c* is the same for the "total" sample. The wedge-shaped envelope lines in (*c*) show the expected distribution if all residuals, read as velocity deviations, are instead due to the spread in the absolute magnitudes with magnitude differences of 0.7 and 1.3 mag, respectively. Any *true* peculiar velocity residuals are buried in the wedge-shaped distribution. True velocity perturbations will be wedge-shaped in the opposite sense. (*b*, *d*) Same as (*a*) and (*c*), but in the direction of the GA for the "bright" and "total" samples, respectively. The envelope lines to the wedge are not drawn again. Note the lack of significant offset of the residuals locally, showing that the "nearby" galaxies are more nearly at rest relative to the (comoving) frame of the Virgo Cluster, than relative to the kinematic (comoving) Machian frame of the CMB, i.e., Fig. 19*b* is fundamentally different from Fig. 18*b*.

Figure 19, similar to Figure 17 but with velocities corrected for Virgocentric infall using $v(220)$, shows the "velocity residuals" for the total sample, but again separated into the two directions. The expected behavior of the errors (if due to distance errors alone) in Figure 19*c* is illustrated for galaxies *outside* the GA direction. The distribution is wedge-shaped, as is required if most of the scatter is due to absolute magnitude spread rather than velocity residuals. The wedge-shaped upper and lower envelopes to Figure 19*c* are what is expected on the premise that the residuals are due entirely to the intrinsic dispersion in the absolute magnitudes. An absolute magnitude difference of ΔM translates to a redshift residual to $5\,\Delta \log v$, or $2.17\,\Delta v/v$. Hence the envelope lines are the loci of constant $\Delta v/v$, i.e., if Δv increases with v, a very unlikely proposition, then the distribution could be a velocity perturbation rather than a variation in absolute magnitude. On the other hand, envelope lines corresponding in this way to *absolute magnitude* spreads (rather than to velocity residuals) of 0.7 and 1.3 mag are shown in Figure 19*c*. Such *spreads* (not dispersions) are the values expected from a dispersion of ~ 0.6 mag for the intrinsic TF relation (Fig. 7).

Figure 19 shows why the detection of individual peculiar motions about a quiet Hubble flow is virtually impossible from the TF relation if the intrinsic dispersion of the method is as high as we have argued in this paper. This is the reason why we are skeptical if any streaming motions have been detected, except for (1) the Virgocentric infall and (2) the almost *bulk* motion of the Local Supercluster toward an apex near Hydra at 495 km s^{-1} amplitude as discussed in § 8.3. These two effects together make up the observed CMB dipole (Tammann & Sandage 1985, Fig. 3), which, of course, is very well determined from the microwave observations of the CMB.

The important point of Figure 19*c* is that the wedge is centered for nearby galaxies at zero velocity residual, and that the mean of the distribution remains near zero velocity residuals, except for the low-weight galaxies beyond $r = 150$ Mpc. Said differently, the mean line through the data is *level*, showing that there is no deviation of the data from a linear redshift-distance relation *outside the GA*.

9. SUMMARY AND CONCLUSIONS

Distances determined from the *I*-band TF method for 1094 southern-sky field Sb–Sd galaxies from the large catalog of

MFB (excluding 261 galaxies which they assign to clusters) have been analyzed. The following conclusions are reached.

1. Naive application of a TF relation such as equation (1) leads to physically unacceptable results that the redshift-to-distance Hubble ratios, calculated for individual galaxies, become functions of redshift, rotational velocity (or line width), and apparent magnitude. The consequence is that, at a given redshift (i.e., distance), H_0 is *multivalued* for different values of v_{rot} and apparent magnitude (Figs. 1 and 2). This contradictory behavior, caused by selection bias in flux-limited samples, is predicted in Papers I and II and is seen here in detail in the MFB data.

Similar internal contradictions are expected in all catalogs of field galaxy distances that are based on statistical relations between absolute magnitude, M, and one or more *observables* such as line width, angular diameter, internal velocity dispersion, surface brightness, apparent magnitude of particular stellar contents, etc., if the samples are flux-limited and if the relation between M and the observed parameter(s) has intrinsic scatter.

2. The bias properties of the naive 1094 TF distances are studied in Spaenhauer diagrams (absolute magnitude versus redshift distance) in Figures 4–6. The assumption of (nearly) linear expansion that is necessary to calculate absolute magnitudes, as supported by external evidence, is consistent with present data to within the statistical and systematic accuracy of the data. The *apparent* scatter of the I-band TF relation is a strong function of v_{rot}, ranging from $\sigma(M) = 0.43$ mag for the fastest rotators to $\sigma(M) = 0.90$ mag for spirals with $v_{rot} < 100$ km s^{-1}; the intrinsic scatter is only marginally smaller. Although the consequences of selection bias are accessible to naive intuition, the values of the intrinsic dispersions at different line widths are so large that their importance and size have generally been underestimated. This underestimate has led to false conclusions concerning possible streaming motions relative to the cosmological flow.

3. A *distance-limited* subsample, cut at different redshifts according to the apparent magnitude flux limits for different line widths (i.e., v_{rot}), defines an *unbiased* TF relation in Figure 7 and equation (4b), similar to that adopted by MFB based solely on Fornax Cluster data. The change of slope for flux-limited samples that is predicted in Paper II, Figure 4 (the slope being significantly flatter for the biased compared with the unbiased sample), is well seen in the data here (Fig. 3*b*).

For reasons implicit in item 2 above, it is not permissible to use equation (4b) for galaxies *beyond the distance at which the flux limit of the catalog cuts into the sample.* Empirical relations between M_I and v_{rot}, redshift, and catalog limit are derived from the Spaenhauer diagrams. Two different catalog limits are considered, viz., $m_I < 12.5$ and the total MFB sample (which is neither complete nor decisively limited by a strict faint catalog limit; most galaxies were chosen by MFB using a lower *angular diameter* as the limit). The resulting triple-entry TF relations (as functions of v_{rot}, redshift, and apparent cutoff magnitude) are shown in Figure 8 for two different assumptions of flux limitation.

4. The empirical TF relation of Figure 8*b* is used to calculate the statistically correct individual distances to be used for each of the sample galaxies for obtaining mean values of such parameters as H_0. A second distance was determined from Figure 8*a* for the galaxies with $I < 12.5$ mag. The two separate distances for galaxies in common with the $I < 12.5$ mag galaxies and the total list will, of course, generally disagree. In either of the two samples with different cutoff apparent magnitudes, the more distant objects must play the role of different proxies for a *different* number of objects that are missed due to selection bias, *because the bias properties of the two samples are different.* The corrections for the brighter ($I < 12.5$ mag) catalog are necessarily larger than for the fainter sample because that subsample is less complete.

5. Our methods of correction for selection bias appear to be simple. However, the simplicity has the advantage over those extant formal analytical discussions in the current literature that depend upon strict adherence of any given sample to rigid selection criteria. We have more direct control of the corrections via the relevant Spaenhauer diagrams. Said differently, the empirical method here is suitable for treating, at least to a considerable extent, incomplete samples and has the advantage of showing the interdependences of the observed parameters such as the variation of the intrinsic dispersion $\sigma(M)$ with v_{rot} and the change in the limiting magnitude of the sample, also with v_{rot}.

However, the one formidable problem not solved at all by the formal methods and not discussed (only mentioned) in Paper I, Paper II, or here is the effect on the bias corrections of *nonuniform* spatial distribution of the sample galaxies. This problem can, however, be treated by proper study of the relevant Spaenhauer diagrams as a function of position in the sky (Paper I, Fig. 11 and the discussion of it) in an obvious way (see the Monte Carlo simulation by Spaenhauer shown as Fig. 2 in Tammann & Sandage 1982).

6. The bias-corrected individual galaxy distances using the total sample define a roughly linear Hubble diagram (Fig. 11*c*; the data for galaxies beyond 140 Mpc are necessarily uncertain). The linearity is even closer for the nearly complete, and therefore more reliable, bright subsample ($I < 12.5$ mag, Fig. 12*b*) away from the direction of the "GA," and is still clearer when the galaxies with $v_{rot} < 100$ km s^{-1} with $\sigma(M) = 0.9$ mag are ignored (Fig. 12*c*). Recovery of the linearity with the output H_0 equal to the input H_0 is required if our bias corrections are valid, because linearity was assumed a priori in the determination of the corrections. Consistency of the final H_0 result with the input H_0 assumption proves the validity of the corrections.

Proof against the circularity of the method comes by showing that the Hubble ratios, h_i, become now independent of redshift, apparent magnitude, and v_{rot} (Figs. 9 and 10), the *physically impossible multivaluedness of H_0 having been removed using the corrections.*

7. The present data with their incomplete sky coverage do not render a decisive test for the Virgocentric infall model, but they are consistent with it.

8. The Hubble diagrams plotted separately for the regions toward and away from the GA show a significant velocity excess in the GA direction for relatively nearby galaxies (i.e., $v \sim 2000$ km s^{-1}). This effect needs further study, but it is not the signature of the putative Great Attractor. In addition, there is a systematic offset of ~ 500 km s^{-1} for the nearer galaxies in the GA direction when the velocities are referred to the kinematic frame of the CMB radiation (Figs. 16 and 17). The velocity offset becomes, if anything, even more obvious, with an amplitude of 650 ± 30 km s^{-1} when the direction is changed from that of the GA to that of the position of the warm CMB pole (Fig. 18), some 30° from the direction of the GA.

The excess velocity decreases with distance and comes close

to zero at 4000 km s^{-1}, arguing against models with an infall into a single GA at $\sim$4500 km s^{-1}, and particularly against infall from its back side, as well as against a very large-scale bulk flow over more than 13,000 km s^{-1} as proposed by Mathewson et al. (1992b) and by Lauer & Postman (1992). Rather, the data support a motion of an incoherent "local bubble" (i.e., there are streaming motions within the bubble—it is not bulk flow *throughout* its entire volume because it has a gradient; it gradually decays to zero at $\sim$4500 km s^{-1} distance). The amplitude (*decaying with distance from us*) and the direction of this motion agree well with the CMB dipole (Fig. 18). The origin of this motion and its systematic and gradual decay with distance are presumably due to the gravitational pull of irregularly distributed galaxies, clusters, and voids *within* a radius of roughly 4000 km s^{-1}. Over still larger scales, the galaxy distribution must be sufficiently homogeneous and isotropic so as not to cause any additional detectable acceleration of the Local Supercluster *relative to the global Machian frame.*

9. The investigation of the systematic errors of TF distances of field galaxies—and in principle of all similarly derived distances by other photometric methods—casts a shadow on claims for large peculiar motions in the field. The accuracy of TF distances, at least from the MFB sample, is limited to 20% even for the fastest rotators, based on the internal dispersion of $\langle\sigma(M)\rangle \sim 0.6$ mag displayed in Figure 7. This shows that *peculiar* motions of individual galaxies that are smaller than $\Delta v/v = 0.20$, based on this distance accuracy, will be smaller than the error of the determination and, therefore, *cannot be warranted.*

Furthermore, apparent streaming motions can be artifically introduced by absent or incorrect bias corrections. Convincing evidence for streaming motions, such as the 500 km s^{-1} motion of the Virgo complex toward the CMB warm pole, can only be given at present by the comparison of two sufficiently separated sky regions for which homogeneous data are available such as those of the MFB sample.

We are grateful to D. S. Mathewson, V. L. Ford, and M. Buchhorn for sending us their extensive MFB catalog in machine-readable form and for encouragement to analyze their important data in this independent way. Financial support of the Swiss National Science Foundation is gratefully acknowledged. Similar support from the US National Aeronautics and Space Administration with a grant through the Space Telescope Science Institute for using the *HST* to determine the Hubble constant is also gratefully acknowledged.

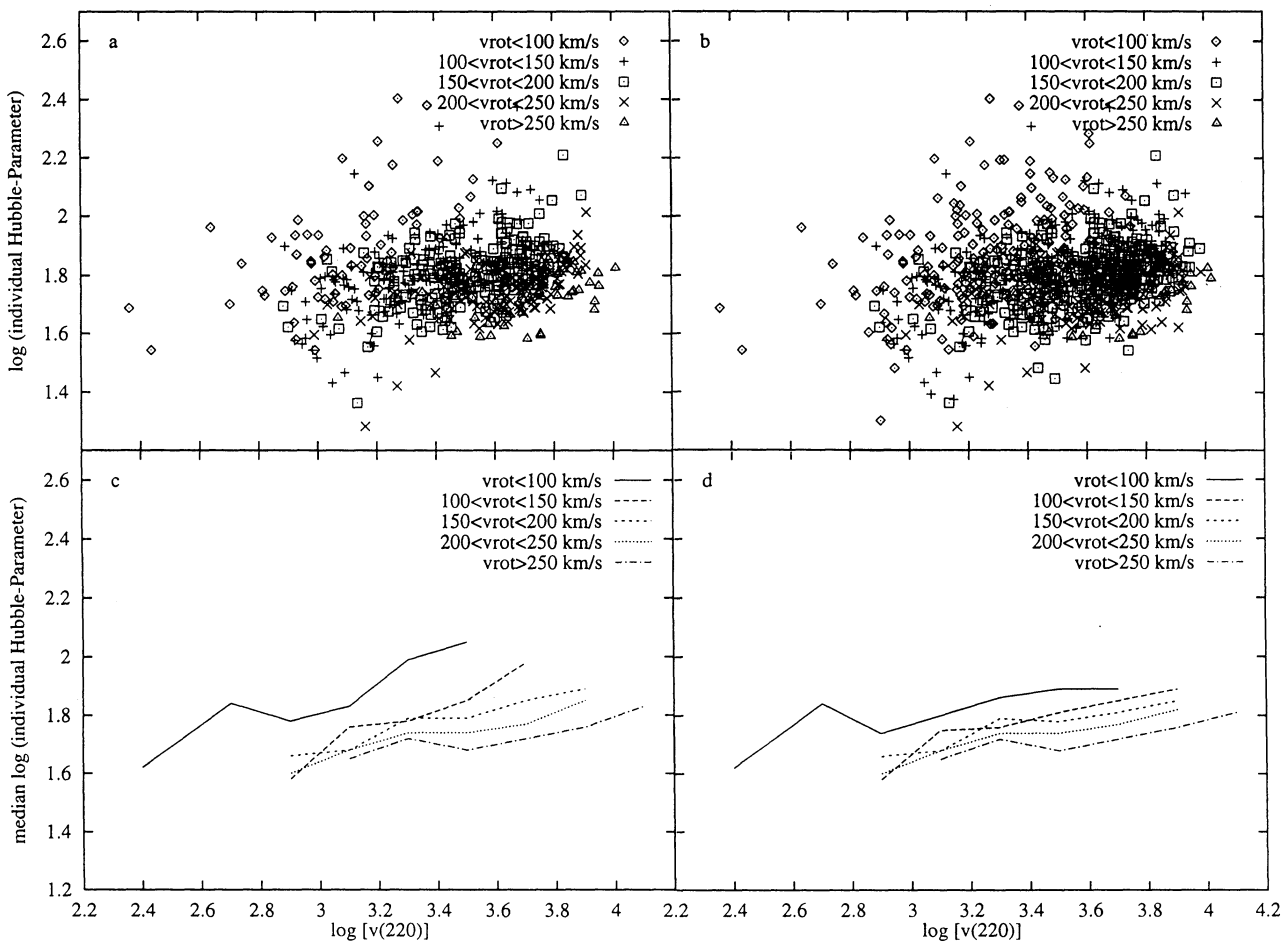

FIG. 20.—Same as Fig. 1, but using $v(220)$ redshifts relative to the Virgocentric kinematic frame rather than v(LG)

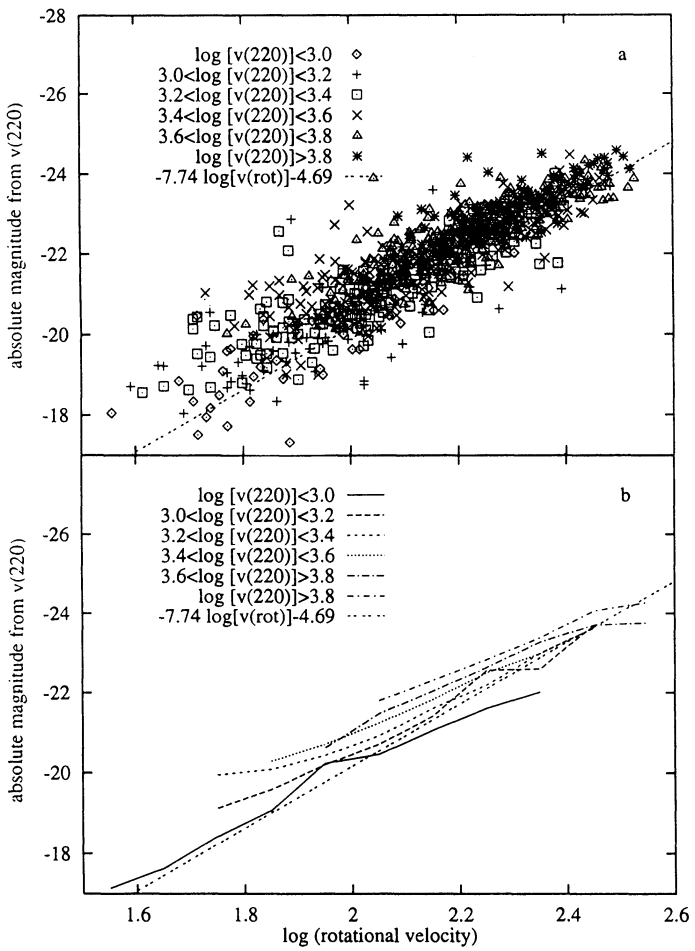

FIG. 21.—Same as Fig. 3, but using $v(220)$ rather than $v(LG)$ redshifts

APPENDIX

Can any of the features of the correlations in this paper be a result of using redshifts relative to the Local Group rather than to the kinematic frame of the Virgo complex? In particular, can the multivaluedness of the derived Hubble constant in Figures 1*c* and 1*d* be eliminated using Virgocentric redshifts? Likewise, can the stacking of the median Tully-Fisher lines in Figure 3*b* at different redshifts be eliminated by using $v(220)$ rather than $v(LG)$ redshifts? A priori, these possibilities would seem highly remote because each of the correlations in Figures 1 and 3 follows the predicted behavior of the bias model of Paper II (Figs. 4, 7, 8, and 16). Nevertheless, a test of the sensitivity of the multivaluedness to the velocity frame is of interest.

Figures 20 and 21 are the same as Figures 1 and 3 of the text, except that they use $v(220)$ redshifts rather than $v(LG)$. The systematics of the diagrams are nearly identical here and in the main text, belying the stated queries concerning possible differences caused by using either the Local Group or the Virgocentric kinematic frame.

REFERENCES

Aaronson, M., et al. 1982, ApJS, 50, 241
Burstein, D., Faber, S. M., & Dressler, A. 1990, ApJ, 354, 18 (BFD)
de Vaucouleurs, G. 1975, in Stars and Stellar Systems, Vol. 9, Galaxies and the Universe, ed. A. Sandage, M. Sandage, & J. Kristian (Chicago: Univ. Chicago Press), chap. 14
de Vaucouleurs, G., & Peters, W. L. 1986, ApJ, 303, 19
Dressler, A. 1988, ApJ, 329, 519
Dressler, A., & Faber, S. M. 1990a, ApJ, 354, 13
Giraud, E. 1985, A&A, 153, 125
———. 1986a, ApJ, 301, 7
———. 1986b, ApJ, 309, 512
———. 1986c, A&A, 174, 23
Hubble, E., & Humason, M. L. 1931, ApJ, 74, 43
Humason, M. L., & Wahlquist, H. D. 1955, AJ, 66, 254
Jerjen, H., & Tammann, G. A. 1993, A&A, 276, 1
Kraan-Korteweg, R. C. 1986a, A&AS 66, 255
Kraan-Korteweg, R. C. 1986b, A Catalog of 2810 Nearby Galaxies (Basel Publ. Ser. No. 18)
Kraan-Korteweg, R. C., Cameron, L. M., & Tammann, G. A. 1986, in Galaxy Distances and Deviations from Universal Expansion, ed. B. F. Madore & R. B. Tully (Dordrecht: Reidel), 65
———. 1988, ApJ, 331, 620
Kristian, J., Sandage, A., & Westphal, J. 1978, ApJ, 221, 383
Lauberts, A. 1982, The ESO/Uppsala Survey of the ESO (*B*) Atlas (Garching: ESO)
Lauer, T. R., & Postman, M. 1992, ApJ, 400, L47
Lynden-Bell, D., Lahav, O., & Burstein, D. 1989, MNRAS, 241, 325
Malmquist, G. 1920, Lund Medd. Ser., No. 22
Mathewson, D. S., Ford, V. L., & Buchhorn, M. 1992a, ApJS, 81, 413 (MFB)
———. 1992b, ApJ, 389, L5
Mould, J. R., Akeson, R. L., Bothun, G. D., Han, M, Huchra, J. P., Roth, J., & Schommer, R. A. 1993, preprint

Pierce, M., & Tully, R. B. 1992, ApJ, 387, 47
Sandage, A. 1972a, ApJ, 173, 485
———. 1972b, ApJ, 178, 1
———. 1975, ApJ, 202, 563
———. 1978, AJ, 83, 904
———. 1986, ApJ, 307, 1
———. 1988a, ApJ, 331, 583
———. 1988b, ApJ, 331, 605
———. 1992, Phys. Scripta, T43, 22
———. 1994a, ApJ, 430, 1 (Paper I)
———. 1994b, ApJ, 430, 13 (Paper II)
Sandage, A., & Hardy, E. 1973, ApJ, 183, 743
Sandage, A., & Tammann, G. A. 1975, ApJ, 196, 313
———. 1981, 1987, A Revised Shapley-Ames Catalog of Bright Galaxies (Carnegie Inst. Washington Publ. 635) (RSA1, RSA2)
Sandage, A., & Tammann, G. A. 1984, in Symp., First ESO-CERN Large Scale Structure of the Universe, Cosmology, & Fundamental Physics, ed. G. Setti & L. Van Hove (Geneva: CERN), 127
———. 1990, ApJ, 365, 1
———. 1993, ApJ, 415, 1
Sandage, A., Tammann, G. A., & Yahil, A. 1979, 232, 352 (STY79)
Shaya, E. J. 1984, ApJ, 280, 470
Strauss, M. A., Yahil, A., Davis, M., Huchra, J. P., & Fisher, K. 1992, ApJ, 397, 395
Tammann, G. A. 1992, Phys. Scripta, T43, 31
Tammann, G. A., & Sandage, A. 1982, in Highlights Astron., Vol. 6, ed. R. M. West (Dordrecht: Reidel), 301
———. 1985, ApJ, 294, 81
Tully, R. B. 1988, Nature, 334, 209
Yahil, A., Tammann, G. A., & Sandage, A. 1977, ApJ, 217, 903